# REVIEW ARTICLE

# Crystal structure, synthesis and characterization of different chromium-based two-dimensional compounds

**Maria Hasan** [a,i,k], **Huy Q. Ta** [a,b,c,d], **Sami Ullah** [a,b,c], **Xiaoqin Yang** [a,b,c,e], **Jingping Luo** [e], **Alicja Bachmatiuk** [f], **Thomas Gemming** [d], **Barbara Trzebicka** [i], **Azhar Mahmood** [g], **Mengqi Zeng** [h], **Lei Fu** [h], **Lijun Liu** [e], **Mark H. Rümmeli** [a,b,c,d,i,j,*]

[a] *Soochow Institute for Energy and Materials Innovations College of Energy, Soochow University Suzhou, 688, Mo Xie Road, Suzhou, Jiangsu Province 215006, China*
[b] *Key Laboratory of Advanced Carbon Materials and Wearable Energy Technologies of Jiangsu Province, Soochow University, Suzhou 215006, China*
[c] *Collaborative Innovation Center of Suzhou Nano Science and Technology, China*
[d] *Institute for Complex Materials IFW Dresden, P.O. Box D-01171, Dresden, Germany*
[e] *School of Energy and Power Engineering Xi'an Jiaotong University, No. 28, Xianning West Road, Xi'an, Shaanxi 710049, China*
[f] *Material Science & Engineering Center Łukasiewicz Research Network – PORT Polish Center for Technology Development Ul, Stabłowicka 147, Wrocław 54-066, Poland*
[g] *School of Natural Sciences, National university of Sciences and Technology, H-12, Islamabad 44000, Pakistan*
[h] *College of Chemistry and Molecular Science, Wuhan University Wuhan 430072, China*
[i] *Centre of Polymer and Carbon Materials Polish Academy of Sciences, M. Curie-Sklodowskiej 34, Zabrze 41-819, Poland*
[j] *Center for Energy and Environmental Technologies VSB-Technical University of Ostrava, 17. Listopadu 15, Ostrava 708 33, Czech Republic*
[k] *NUTECH School of Applied Sciences & Humanities, National University of Technology, Islamabad 42000, Pakistan*

**Abstract** The field of two dimensional (2D) materials experienced a surge of discoveries after the isolation of graphene. Among these, the transition metal compounds of Molybdenum and tungsten have been the most extensively studied materials after graphene. More recently, their group member chromium has only recently come to the limelight after the discovery of its exciting magnetic properties. As such the body of work surrounding 2D chromium-based materials is growing. Here, we

---

\* Corresponding author.
 E-mail address: m.ruemmeli@ifw-dresden.de (M.H. Rümmeli).
Peer review under responsibility of King Saud University.

**ELSEVIER**   **Production and hosting by Elsevier**

present an up-to-date summary of the chromium 2D materials showing the latest advances in their experimental synthesis, characterization and the applications of 2D Chromium-based compounds. Finally, we conclude with a perspective on the future of 2D chromium-based materials. We believe that this study will be helpful to understand the field of chromium-based 2D compounds.

## 1. Introduction

The isolation of graphene generated a new world of two dimensional (2D) materials. The interest in different 2D materials is driven by the virtue of their semiconducting, semi-metallic, insulating, magnetic and numerous other properties that make these materials suitable candidates for numerous different and exciting applications (Khan et al., 2019; Chhowalla et al., 2013). Moreover, these systems can yield Mott insulators, superconductivity, and charge density waves (Gibertini et al., 2019). Today the predicted number of the 2D layered materials has grown to over 5600, of which more than 1800 would be either potentially or easily exfoliated (Ares and Novoselov, 2021). The ever-growing size of the 2D library stresses the need to study the different families constituting the 2D materials in detail with regard to their properties, structure, synthesis methodologies and advanced characterization so as to reap their benefits to the fullest.(See Tables 1 and 2).

Cr is a transition metal in Group 6 of the periodic table (Fig. 1). It can exist in various oxidation states ranging from $-2$ to $+6$ but the most stable is $+3$ (Samadi et al., 2018). In its elemental or uncombined state, chromium is antiferromagnetic at room temperature (Koroleva et al., 2009;153:012057.). Layered as well as non-layered compounds are prominent members of chromium family. Nevertheless, this member of the 2D material family has been long overshadowed by its neighbors i.e., Molybdenum and tungsten which led to the relatively late realization of the unconventional properties of chromium-based 2D materials such as giant tunneling magnetoresistance and a wide range of magnetic behaviors (Song et al., 2018; Gong et al., 2017; Chu et al., 2019; Ta et al., 2020). Still, most of the available scientific literature on chromium-based materials discuss these under the umbrella of contemporary magnetic compounds. A detailed literature, to the best of our knowledge, focusing on chromium-based 2D materials, their crystal structure, properties, and fabrication strategies is missing.

This review article provides a detailed study of chromium-based 2D material and compiles state of the art developments in this 2D family with particular emphasis on the material sub-classes and their crystal structure, and, their synthesis and characterization techniques. At the end we review potential applications of these 2D compounds in fields such as spintronics, biomedicine, and fuel cells are discussed in brief. Finally, future perspectives in the field of the chromium 2D family area also provided. First, we start with the different 2D compounds of chromium that it forms with other elements (Fig. 1),

First, we start with the different 2D compounds that chromium forms with other elements in the periodic table. The compounds are categorized using the name of the family to which the elements belong in the periodic table.

## 2. Chromium Trihalides, CrX$_3$ (X = F/Cl/Br/I)

Chromium Trihalides (CrX$_3$) are van der Waals layered compounds that are semiconducting in nature. The ferromagnetic semiconducting property of the family was discovered in 1960 while studying CrBr$_3$, though the CrX$_3$ family has still not been well studied. In CrX$_3$ crystals, the Cr atom exists in $+3$ oxidation state. Cr ions are arranged in a honeycomb lattice in an edge-sharing octahedral geometry where each ion is further coordinated by six halide (X$^-$) ions (McGuire et al., 2015) Thus, CrX$_3$ layers stack with van der Waals gaps separating these layers. Consequently, the resultant structure is determined by the stacking sequence and relative distance between the layers (McGuire et al., 2015). Notably, in this family CrF$_3$ has hardly been studied in the literature and, it has been experimentally noted that it adopts the R$\bar{3}$c phase (Knox, 1960). At low temperature all CrX$_3$ (X = Cl, Br, or I) except CrF$_3$, adopt a rhombohedral BiI$_3$ like crystal system (space group R$\bar{3}$) that upon warming transforms into a monoclinic AlCl$_3$ type system having C2/m space group(Zhang et al., 2015). However, at room temperature the preferred geometry for CrCl$_3$ and CrI$_3$ is monoclinic while CrBr$_3$ has a rhombohedral crystal system. First-principle, calculations predict all CrX$_3$ (X = F, Cl, Br, or I) without exception to have a smaller cleavage energy than graphite; hence, they can be exfoliated as atomically thin 2D materials from their bulk phases (Liu et al., 2016). Moreover, their respective mono layers have high in-plane stiffness, suggesting that they do not curve easily and are stable(Zhang et al., 2015). At ambient temperature and pressure, CrCl$_3$ and CrBr$_3$ have relatively greater air stability than CrI$_3$ (Zhang et al., 2019; Kazim et al., 2020).

CrX$_3$ have strong intraplanar ferromagnetic coupling; but their nature varies (McGuire et al., 2015; Zhang et al., 2015). For example, in CrCl$_3$ the interplanar coupling is antiferromagnetic with a Neel temperature of 16.8 K. Even so, CrCl$_3$ layers can be aligned ferromagnetically in the direction of an externally applied magnetic field of only a few kilooersted (McGuire et al., 2015). On contrary, in CrBr$_3$ and CrI$_3$, the layers stack ferromagnetically with Curie temperatures (Tc) of 37 and 61 K, respectively. Unlike CrCl$_3$, the Cr ions in CrBr$_3$ and CrI$_3$ have moments directed normal to the CrX$_3$ layers and more magnetic anisotropy is observed in their magnetically ordered state (McGuire et al., 2015; Zhang et al., 2015). CrBr$_3$ bilayers retain ferromagnetic behaviors. Contrary to this, CrI$_3$ bilayer is antiferromagnetic (Zhang et al., 2019; Huang et al., 2017). Nevertheless, a large linear magnetoelectric effect is observed in the bilayer CrI$_3$, which makes its magnetism electrically controllable(Jiang and Shan, 2018). Besides,

**Table 1** Crystal structure and space groups of the chromium-based 2D binary compounds.

| Formula | Crystal Structure | Space group |
| --- | --- | --- |
| CrCl$_3$, CrI$_3$ | iMonoclinic | C2/m |
| CrBr$_3$, Cr$_2$S$_3$ | Rhombohedral | R3$^-$ |
| CrO$_2$ | Tetragonal | P42/mnm |
| Cr$_x$-Se$_y$ | Hexagonal | P63/mmc |
| CrN | Cubic | Pm3$^-$m |
| CrP, CrAs, CrSb | Orthorhombic | Pnma |
| Cr$_3$P | Tetragonal | I4$^-$ |

**Table 2** Summary of the 2D chromium-based compounds with the production methods, morphology and magnetic properties.

| Method | Compound | VdW, n-VdW | Substrate | Precursors | Layers No. | Morphology | Properties | Ref |
|---|---|---|---|---|---|---|---|---|
| CVD | 2D $CrS_2$ | Layered | Si | S vapor and Cr | Mono and multilayer | nanoflakes | AFM | (Habib et al., 2019; Wang et al., 2018) |
| CVD | $Cr_2S_3$ | n-VdW | Mica | S and $CrCl_2$ | Monolayer | nanoflakes | AFM | (Zhou et al., 2019;29(3):1805880.; Cui et al., 2020;32(4):1905896.) |
| CVD | $CrO_2$ | | $TiO_2$ (Kang et al., 2015) | $CrO_3$ | 500 Å-1.2 μm | Thin Films | FM | (Li et al., 1999) |
| APCVD | $CrO_2$ | | TiO2(Kang et al., 2015) (Alam et al., 2017) (Constantin et al., 2004) (0 0 1) | $CrO_3$ | | Thin Films | | (Ishibashi et al., 1979) |
| LPCVD | $CrO_2$ | | $TiO_2$ (Kang et al., 2015); (0 0 1) (Alam et al., 2017) | $CrO_3$ | | Thin Films | | (Aguilera et al., 2013) |
| CVD | $CrO_2$ | | $TiO_2$ (Alam et al., 2017) | $CrO_3$, $Cr_8O_{21}$ | | Thin Films | | (Ivanov et al., 2001; Bullen and Garrett, 2002) |
| APCVD | CrSe | Non layered | Mica | Se and $CrCl_3$ | Monolayer | nanoflakes | FM | (Zhang et al., 2019) |
| MBE | $Cr_2Se_3$ | Non layered | $Al_2O_3$(0001) Si(Constantin et al., 2004) | Cr and Se | multilayer | Thin Films | AFM | (Roy et al., 2020; Ningrum et al., 2020) |
| MBE | $CrTe_2$ | VdW | GaAs (Constantin et al., 2004)B | Cr and Te | Few layer | Thin Films | FM | (Sun et al., 2021;11(3):035138.) |
| MBE | $Cr_3Te_4$ | VdW | pyrolytic graphite | Cr and Te | Monolayer | Thin Films | FM | (Chua et al., 2021) |
| APCVD | $Cr_2S_3$ | Non layered n-VdW | Mica | S and $CrCl_3$ | Monolayer | Thin Films | FM | (Chu et al., 2019) |
| CVD | $CrS_2$, $CrSe_2$, $CrTe_2$ | | sapphire | Cr and Au alloy, chalcogen vapors | Monolayer | Thin Films | FM | (Shivayogimath et al., 2019) |
| PLD | $CrO_2$ | | MgO (Kang et al., 2015) | Cr and $O_2$ | Multilayer | Thin Films | | (Heinig et al., 2007) |
| CVT | $CrPS_4$ | VdW | – | Cr, P, and S powders | – | Thin Films | Capacitors | (Lee et al., (CrPS 4). 2018) |
| WS | Cr/rGO and MnO | | – | $Mn(NO_3)_2 \cdot 4H_2O$ and $Cr(NO_3)_3 \cdot 4H_2O$ | – | Powder | Electro-catalyst | (Khan et al., 2019) |
| AT | $Cr_2Ge_2Te_6$ | | 260-nm-thick $SiO_2$/Si | Bulk $Cr_2Ge_2Te_6$ | Bilayer | Thin Flakes | | (Gong et al., 2017) |
| ME | $CrI_3$ | | $SiO_2$/ Si substrate | Bulk $CrI_3$ | Monolayer | nanoflakes | SM | (Huang et al., 2017) |
| ME | $CrI_3$ | | $SiO_2$/ Si substrate | Bulk $CrI_3$ | Bilayer | nanoplatelets | | (Zavabeti et al., 2020) |
| ME | $CrSiTe_3$ | | $SiO_2$/ Si | bulk | Mono and few layer | nanosheets | FM | (Lin et al., 2016) |
| EB | NP CrO | | Graphene | $Cr(C_5H_7O_2)_3$ | | Membrane | | (Ta et al., 2020) |
| EB | Cr | | Free Standing | $Cr(C_5H_7O_2)_3$ | Monolayer | Membrane | AFM | (Ta et al., 2020) |

VdW = Vander Waal, n-VdW = Non vander Waal.
Abbreviations in methods: MBE = Molecular Beam Epitaxy, PLD = Pulsed laser deposition, CVT = Chemical Vapor Transport, WS = Wet synthesis, ME = Mechanical Exfoliation, EB = Electron Beam, HPD = High pressure decomposition, AT = Adhesive tape.
Abbreviations in Properties: FM = Ferromagnetic, AFM = Antiferromagnetic, SM = Semiconductor.

**Fig. 1** Periodic table highlighting the different 2D combinations of Cr with other elements.

density functional theory studies predicts that $CrX_3$ (X = Cl, Br, and I) can undergo a phase transition from a ferromagnetic to an antiferromagnetic state upon application of compressive strain(Webster and Yan, 2018). The structural information of monolayer $CrX_3$ (X = Cl, Br, and I) is shown in Fig. 2a.

### 3. Chromium chalcogenides

Chromium chalcogenides are a sundry family, that can exist in different stoichiometric compositions. However, the most common ones are $CrY_2$, $Cr_2Y_3$, and $Cr_3Y_4$. In $CrY_2$ (where Y represent O/S/Se or Te). Starting with chromium dioxide ($CrO_2$), it is a metallic ferromagnetic oxide that crystallizes in the tetragonal rutile structure (P42/mnm space group). Here Cr positions at the center of an octahedral cage that is formed by six oxygen atoms (Cai et al., 2013; Sousa et al., 2007). The electrical resistivities of single-crystal $CrO_2$ and epitaxial thin films are reported to be approximately 250 and 400 $\mu\Omega$ cm, respectively, at room temperature while its curie temperature has been reported as 395 K (Cho, 2003). In different studies conducted, a Dirac electronic phase has been predicted at the interface in thin films and superlattice configurations of $CrO_2$ and $TiO_2$ heterojunctions (Cai et al., 2013; Wang et al., 2015). $CrO_2$ stability is significantly influenced by temperature and oxygen pressure during its preparation. $CrO_2$ is metastable at atmospheric pressure, it decomposes into an insulating antiferromagnetic $Cr_2O_3$ when it is heated above 200 °C (Audier et al., 2010). The other competing oxides are $CrO_3$, $Cr_2O_5$, and $Cr_3O_4$; but $Cr_2O_3$ is the most stable among these (a = 4.951 Å; c = 13.566 Å; space group: R3c) (Ivanov et al., 2001; Rabe et al., 2001).

Coming to the next member of chromium dichalcogenides, Chromium disulphide ($CrS_2$) is a material possessing piezoelectric coupling, valley polarization, and dependent intrinsic magnetic properties (Habib et al., 2019; Zhuang et al., 2014). Like other VI transition metal dichalcogenides (TMDs), the Cr layer in $CrS_2$ is also sandwiched between two S layers. Based on the coordination number of Cr, $CrS_2$ can adopt three different phases: Viz 2H (or trigonal prismatic), 1 T (or octahedral geometry), and 1 T' (or distorted octahedral geometry). In the 2H phase (Fig. 2b top), Cr and S atoms form ABA stacking, where A and B denote the S and Cr atoms, respectively. The 1 T-$CrS_2$ (Fig. 2b bottom) is characterized by the ABC sequence, where one S layer (C) is shifted compared to the others. The 1 T' phase of $CrS_2$ arises from the dimerization of the 1 T phase. Like $MoS_2$, 2H $CrS_2$ mono-layer is semiconducting, whereas 1 T-$CrS_2$ mono-layer is metallic (Habib et al., 2019; Zhuang et al., 2014). 1 T'-$CrS_2$ is semi-metallic with an approximate bandgap of 10 meV (Habib et al., 2019). Theoretical calculations show that 2H $CrS_2$ is a nonmagnetic semiconductor; whereas 1 T' $CrS_2$ and 1 T exhibit 2.206 and 0.531 $\mu B$ magnetic moment per Cr atom, respectively. Moreover, it has been reported that 1 T-$CrS_2$ switches from antiferromagnetic to ferromagnetic property when going from a monolayer to bilayer or thicker $CrS_2$ (Wang et al., 2018). $CrS_2$-based field-effect transistors exhibit p-type behavior (Habib et al., 2019).

Progressing the discussion to chromium tellurides; these exhibit ferromagnetic properties (Dijkstra et al., 1989; Yamaguchi and Hashimoto, 1972; Wang et al., 2018). Monolayer $CrTe_2$ is a 2D ferromagnet; though, it is metastable in bulk, and its multilayers decompose into intercalating compounds i.e., preferably $Cr_3Te_4$ or $Cr_2Te_3$ (Lasek et al., 2020).
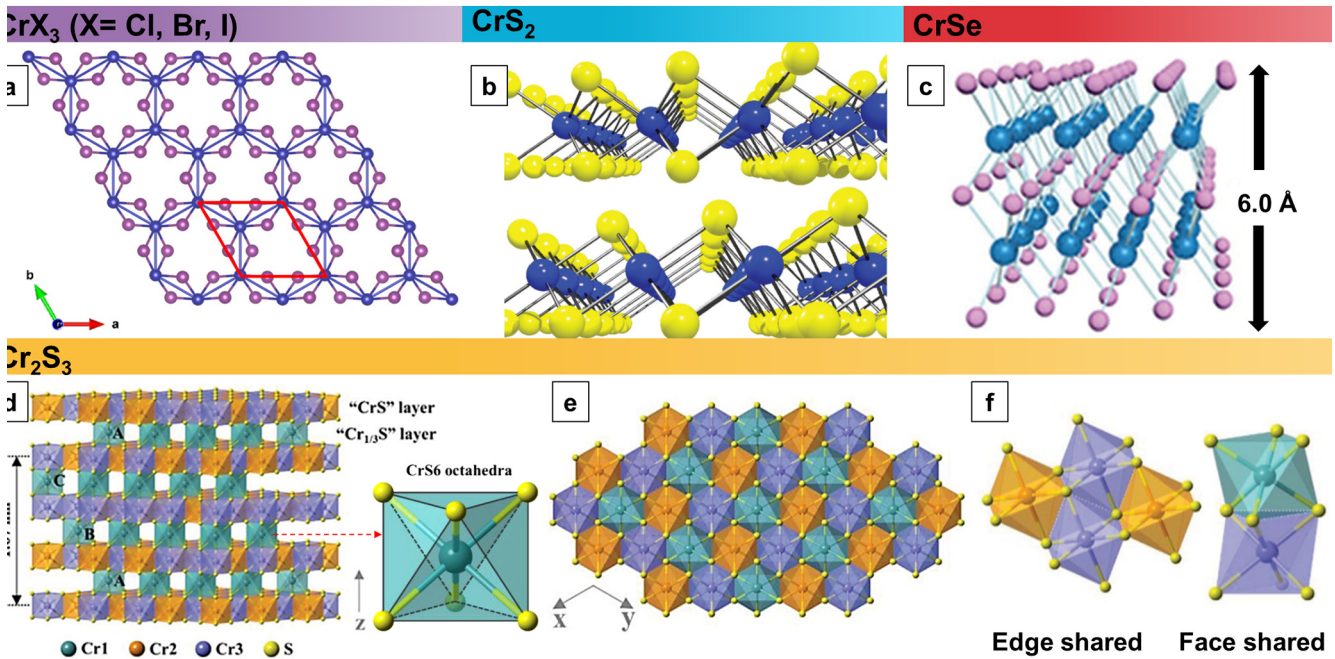
**Fig. 2** **(a)** Atomistic structure of monolayer $CrX_3$ (X = Cl, Br, or I). a) Top view of a single layer. Reproduced with permission from Ref. (Webster and Yan, 2018) Copyright 2018, American Physical Society. **(b)** Single-layer $CrS_2$ with 2H (top) and 1 T (bottom) structures. Cr and S are represented by the blue and yellow balls, respectively. Reprinted from Ref. (Zhuang et al., 2014) [APPLIED PHYSICS LETTERS 104, 022,116 (2014)] with the permission from AIP Publishing **(c)** Structural model of a CrSe crystal. Reproduced with permission from Ref. (Zhang et al., 2019). Copyright 2019, John Wiley and Sons **(d-f)** Structural models of rhombohedral $Cr_2S_3$. d) Perspective view and e) top view showing the periodic stack of the fully filled "CrS" layer and partially filled "Cr1/3S" layer. The stacking along the z-direction with an A–B–C sequence induces a rhombohedral $Cr_2S_3$. Blue, orange, and purple balls represent Cr atoms with different occupancies in the structure. Yellow balls denote S atoms. The entire structure is composed of $CrS_6$ octahedras, in which (f) interlayer octahedras are connected by faces, whereas the intralayer octahedras are connected by edges. Reproduced with permission from Ref. (Zhou et al., 2019;29(3):1805880.). Copyright 2018, John Wiley and Sons.

The 1 T-$CrTe_2$ phase can be successfully grown only as a monolayer, where the hexagonal Cr planes are sandwiched between Te layers. The $CrTe_2$ layers stack via van der Waals interactions (Lasek et al., 2020; Sun et al., 2021;11 (3):035138.; Otero Fumega et al., 2020). The d electrons of Cr provide a non-zero magnetic moment and the emergence of a charge density wave phase in monolayer 1 T-CrTe2, indicating that this phase is the ground state at any strain value in the single-layer limit (Otero Fumega et al., 2020). Moreover; monolayers of $Cr_3Te_4$ and $Cr_2Te_3$ with room-temperature ferromagnetism and improved Tc, respectively, have also been reported (Chua et al., 2021; Lee et al., 2021). Compared to S and Se, Te has a larger ionic radius that results in the broadening of its d orbitals. Therefore, transition metal tellurides have a smaller bandgap, which makes these compounds a better option for optoelectronic applications in the infrared wavelength range (Su et al., 2019).

Among the chromium chalcogenides of $Cr_2Y_3$ stoichiometry, rhombohedral $Cr_2S_3$ (Fig. 2d-f) is an extensively studied antiferromagnetic, non-van der Waals material with a Neel temperature of ≈120 K, which is significantly greater than the Tc of $CrI_3$, making it a suitable candidate for future magnetic applications (Zhou et al., 2019;29(3):1805880.). It was established that the conductive properties of $Cr_2S_3$ vary with increasing thickness from p-type to ambipolar and then to n-type (Cui et al., 2020;32(4):1905896.). Similarly, Cr–Se is another member of this category occurring in diverse stable

stoichiometries such as $Cr_7Se_8$, $Cr_5Se_8$, $Cr_3Se_4$, $Cr_2Se_3$, and CrSe. All these compounds have a hexagonal NiAs structure (space group P63/mmc) (Roy et al., 2020), with have varying magnetic properties (Polesya et al., 2013). For instance, CrSe is a non-van der Waals material with clear ferromagnetic properties at temperatures below 280 K (Ningrum et al., 2020; Zhang et al., 2019). On the contrary, $Cr_2Se_3$ is an antiferromagnet with a Neel temperature of 43 K (Adachi et al., 2007). The crystal structure of CrSe could be considered as two $CrSe_2$ layers stacked together by a layer of Se atoms; as shown in Fig. 2c.

## 4. Chromium pnictides

Chromium can form binary compound with pnictides (the nitrogen family). Theoretically, all hexagonal monolayers of chromium pnictides CrZ (Z = P, As, Sb or Bi) have been predicted to be dynamically stable and they possess half-metallic ferromagnetic characteristics with the Tc above the room temperature as well as spin-dependent transport properties (Mogulkoc et al., 2020;102(2):024441.).

Starting with chromium nitride (CrN), it exhibits good corrosion, wear, and oxidation resistance. It has a face-centered cubic lattice at room temperature with paramagnetic properties. Nonetheless, the structure undergoes orthorhombic distortion and becomes an antiferromagnet below the Neel

temperature (273 K) (Mogulkoc et al., 2020;102(2):024441.; Era et al., 2005). In CrN films, there is a predominant phase transformation to the hexagonal crystal structure of $Cr_2N$ at temperatures above 700 °C. However, at temperatures below 550 °C, the films formed were polycrystalline (Gharavi et al., 2018;51(35):355302.). It is concluded that this transition at lower temperatures is a stress-relaxation-induced phase transformation (Chen, 2003). CrN is semiconducting, having a seebeck coefficient of $-230$ $\mu VK^{-1}$ at 600 K and a high power factor of $5.0 \times 10^{-3}$ $Wm^{-1}$ $K^{-2}$ for single-phase CrN at room temperature (Gharavi et al., 2018;51(35):355302.). In contrast to CrN, $Cr_2N$ is metallic, with a seebeck coefficient of few $\mu VK^{-1}$ and thermal conductivity of 12 W $m^{-1}$ $K^{-1}$ at room temperature, which is approximately 4.0 W $m^{-1}$ $K^{-1}$ for CrN (Gharavi et al., 2019). The phase shift between CrN and $Cr_2N$ can be controlled by the deposition temperature and partial pressure of the nitrogen gas flow (Hones et al., 1997).

Chromium phosphide (CrP) is yet another member of this family that having orthorhombic lattice. It is thermally stable, metallic, and has anti-corrosive and oxidation-resistant properties (Liu et al., 2019; Motojima and Higashi, 1985). Chemically resistant and conductive CrP films have been produced using chemical vapor deposition (CVD) (Blackman et al., 2004). Similarly, another stoichiometry, $Cr_3P$ (tetragonal), has also been produced using CVD. These phosphides have potential applications as protective coatings for metals prone to oxidation and in catalysis (Motojima and Higashi, 1985; Blackman et al., 2004).

Coming to the next member of this family, chromium arsenide (CrAs): it has been found to possess superconductive behavior under external pressure. It has an orthorhombic MnP-type crystal structure at ambient temperature (Nigro et al., 2020). Soon after the discovery of CrAs, bulk superconductivity at room temperature was discovered in $K_2Cr_3As_3$ (Bao et al., 2015). Similarly, three additional superconductors in $A_2Cr_3As_3$ stoichiometry, where A can be Na, Rb, or Cs, have also been synthesized (Mu et al., 2018; Tang et al., 2015). This family of unconventional superconductors have a quasi-one-dimensional crystal structure with infinite $[(Cr_3\text{-}As_3)^{2-}]_\infty$ linear chains of double-walled sub-nanotubes interconnected by A + ions (Noce, 2020). The family is still under further investigation for correlation between electronic properties and the reduced dimensionality.

Progressing further in the family; the theoretical investigations on the magnetic properties and electronic structures of CrSb are very rare. Although, the electronic structure of CrSb has been compared with those of CrP and CrAs having a MnP-type structure (Polesya et al., 2013; Ito et al., 2007). Similarly, two dimensional chromium bismuthate (CrBi), is also only theoretically studied member of the family that has been predicted to have a room temperature Ising ferromagnetism with tunable magneto-optical response (Mogulkoc et al., 2021).

## 5. Chromium-based ternary compounds

Among the ternary compounds of chromium, layered tellurides with the stoichiometric formula $CrXTe_3$ (X = Si, Ge, Sn, Pb) have been extensively studied. These materials have attracted significant research interest as potential candidates for two-dimensional magnets due to their range of magnetic characteristics. For instance, monolayer $CrSiTe_3$ is a robust 2D ferromagnetic semiconductor that forms the basis for spintronics, and it is a good example of a layered telluride with pairs of silicon atoms. It is formed from stacks of Te–(Cr, Si)–Te sandwich layers. Each layer has a $Si_2Te_6$ (ethane-like group) with two Cr ions inserted between two layers of Te planes, leading to a van der Waals gap of approximately 3.3 Å. The Cr ions form a honeycomb sublattice with Si pairs at the center of the hexagons (Casto et al., 2015; Lin et al., 2016; Ouvrard et al., 1988). The crystal structure of $CrSiTe_3$ is shown in Fig. 3a (Lin et al., 2016). Using the Heisenberg model, it has been predicted that the Tc of the single-layer $CrSiTe_3$ would significantly shift to higher temperatures compared to its bulk form, and it would increase further when the $CrSiTe_3$ layers are strained (Casto et al., 2015; Lin et al., 2016; Ouvrard et al., 1988; Li and Yang, 2014; Chen et al., 2015). Some Other theoretical calculations predict that the monolayer $CrSiTe_3$ should be antiferromagnetic when the significance of second-and third-order exchange interactions are considered (Sivadas et al., 2015). However, experimental confirmation still lacks.

Similarly, $CrGeTe_3$ is a layered ferromagnetic telluride is structurally similar to $CrSiTe_3$; except for that its Tc ($\sim$61 K) is relatively higher than that of $CrSiTe_3$ (32 K) (Li and Yang, 2014; Tian et al., 2016). Besides, the spins point lies along the c-axis in both materials (Casto et al., 2015; Zhang et al., 2016). The layers in $CrGeTe_3$ were bound together more tightly as compared to those in $CrSiTe_3$. Thus, $CrGeTe_3$ has a smaller band gap of 3.27 °A compared to $CrSiTe_3$ (3.32 °A), resulting in a shrinking effect of the lattice parameter c from $CrSiTe_3$ to $CrGeTe_3$ (Li and Yang, 2014); which could lead to a transition of the magnetic mechanism from 2D to 3D. Additionally, $CrGeTe_3$ has been reported as a substrate for inducing an anomalous quantum Hall effect in the topological insulator $Bi_2Te_3$ (Alegria et al., 2014).

The single layer of $CrSnTe_3$ has been predicted to be mechanically and dynamically stable (Fig. 3b) (Zhuang et al., 2015). The formation energy of $CrSnTe_3$ is higher compared to those of $CrSiTe_3$ and $CrGeTe_3$, revealing that it exhibits the strongest interlayer coupling, indicating that the magnetism of $CrSnTe_3$ should be closer to that of the 3D-Ising model (Lin et al., 2017). Yet to date, single-crystalline $CrSnTe_3$ has not been experimentally isolated. Similarly, CrPbTe3 has only been predicted to exist. Its cohesive energy is negative and similar to 2D silicone that suggest that the material should be thermodynamically stable once synthesized (Khan and Hong, 2020).

Chromium thiophosphate ($CrPS_4$) is another 2D-layered ternary compound of chromium (Fig. 3c). It is semiconducting with an energy gap of 0.166 eV and an antiferromagnetic transition temperature of 36 K. $CrPS_4$ crystallizes into a monoclinic crystal system where its lattice has puckered hexagonally close-packed sulfur layers parallel to the bc plane. The Cr and P atoms are coordinated in distorted octahedral and tetrahedral interstices, respectively, by S atoms. A large Vander Waal gap exists between the S layers along the c-axis in the bulk (Pei et al., 2016). The in-plane anisotropy and peculiar metamagnetic transitions make few-layered $CrPS_4$ flakes a promising candidate for studying 2D magnetism and exploring
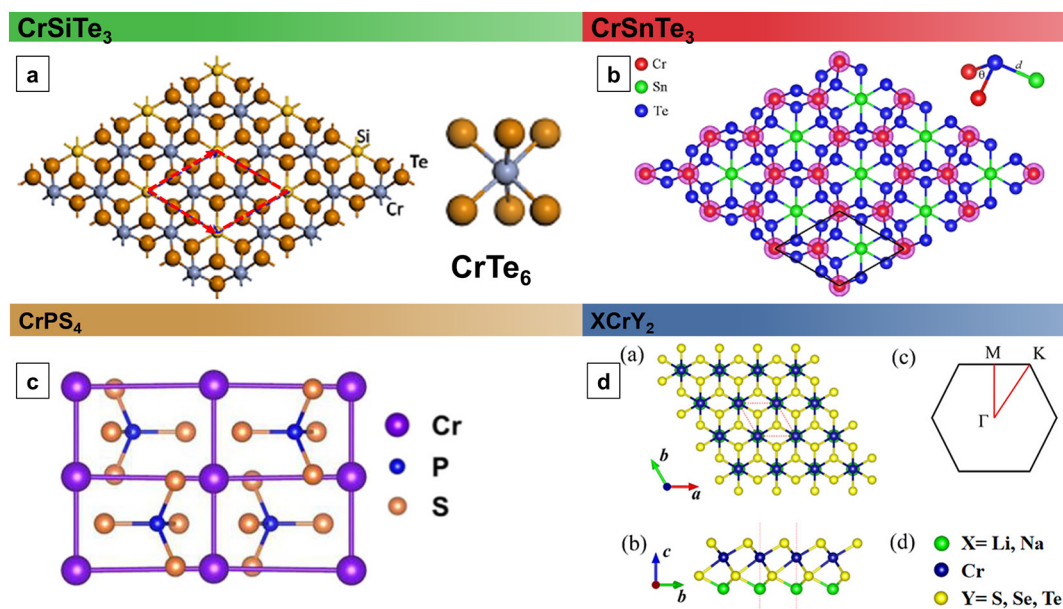
**Fig. 3** **(a)** Top views of the atomic structure of a 2D CrSiTe$_3$ monolayer. A unit cell is indicated by the red dashed line. The local atomic structure around Cr, a distorted CrTe$_6$ octa-hedron, is shown on the right. Reproduced with permission from Ref. (Chen et al., 2015). Copyright 2015, Elsevier. **(b)** Top view of a single-layer CrSnTe$_3$ structure. The solid black line denotes a unit cell of the single-layer CrSnTe$_3$. The spin charge density is also shown with an isosurface of 0.025 e/°A3. Reprinted figure with permission from Ref. (Zhuang et al., 2015) Houlong L. Zhuang, Yu Xie, P. R. C. Kent, and P. Ganesh, PHYSICAL REVIEW B Computational discovery of ferromagnetic semiconducting single-layer CrSnTe$_3$ 92, 035,407 (2015) Copyright 2015, American Physical Society **(c)** Schematic illustration of the atomic structure of CrPS$_4$. Reproduced with permission from Ref. (Lee et al., (CrPS 4). 2018). Creative Commons CC BY license **(d)** a) Top and b) side views of the relaxed structures of XCrY$_2$ (X = Li and Na; Y = S, Se, and Te) FMS monolayers. c) Brillouin zone of the XCrY$_2$ monolayers. d) The green, purple, and yellow spheres represent alkali metals, Cr, and Y atoms, respectively. Reproduced with permission from Ref. (Xu et al., 2020). Open Access, American Chemical Society.

synaptic devices as well as their applications in neuromorphic computing (Lee et al., 2018; Peng et al., 2020; Cao et al., 2021).

Similarly, CrMAs (M = Ni or Rh) is another family of 2D chromium-based ternary compounds with Fe$_2$P-type crystal structures, where Cr atoms occupy pyramidal sites, whereas Ni and Rh are present at tetrahedral sites. The nature of the atoms present at tetrahedral sites is crucial in deciding the magnetic property of the compounds. For instance, CrNiAs is known as a ferromagnet with a Tc of 193 K (Nylund et al., 1972). In contrast, CrRhAs is an antiferromagnet with a Neel temperature of 165 K (Ohta and Kanomata, 1990; Ohta et al., 1995).

Monolayer alkali-based chromium chalcogenides, XCrY$_2$ (X = Na and Li Y = Se, S, and Te), is a theoretically proposed class of ferromagnetic semiconductors (Fig. 3d) (Xu et al., 2020). First-principles calculations predicted the separation of XCrY$_2$ from their bulk crystals to be possible via exfoliation. Using the Ising and Heisenberg models, LiCrSe$_2$, NaCrTe$_2$, and NaCrSe$_2$ were established to exhibit direct band gaps and ferromagnetic ground states with high magnetic curie temperature (Tc). Moreover, the spin–orbit coupling (SOC) effects might significantly change the effective mass of the holes, leading to a higher hole mobility. Furthermore, the high potential difference ($\Delta$V greater than 1.23 eV) between the lower and upper surfaces of the XCrY$_2$ monolayer is suitable for photocatalytic water splitting applications (Xu et al., 2020; Kumari et al., 2021).

## 6. Mono layer chromium

Owing to their high aspect ratio, large specific area, and unsaturated surface coordination, the freestanding 2D elemental nanosheets of atomic thickness have always been of distinct advantages over their bulk counterparts (Ling et al., 2015). Contrary to van der Waals layered 2D materials, metallic bonding systems support close packed structures, due to which monolayer free standing metallic sheets are challenging, though recent theoretical and experimental studies indicate their existence.

Chromium is archetypal antiferromagnet material, with an incommensurate spin-density wave (SDW). Moreover, it is the only solid having antiferromagnetic ordering below (and at) room temperature that can form paramagnetic ordering above 38 °C. The 3d character of this metal is of fundamental importance, considered the absence of antiferromagnetism in Mo and W. Apart from the rare earths and actinides, in which the localized f electrons are responsible for the magnetic nature, the three elemental antiferromagnets are indeed all 3d metals: i.e., Cr, α-Mn, and γ-Fe (Fawcett, 1988). Antiferromagnetic materials can generate large magneto transport effects, display ultrafast dynamics, they are robust against perturbation due to magnetic fields and produce no stray fields. Thus, Antiferromagnetic materials could represent the future of spintronic applications (Baltz et al., 2018).
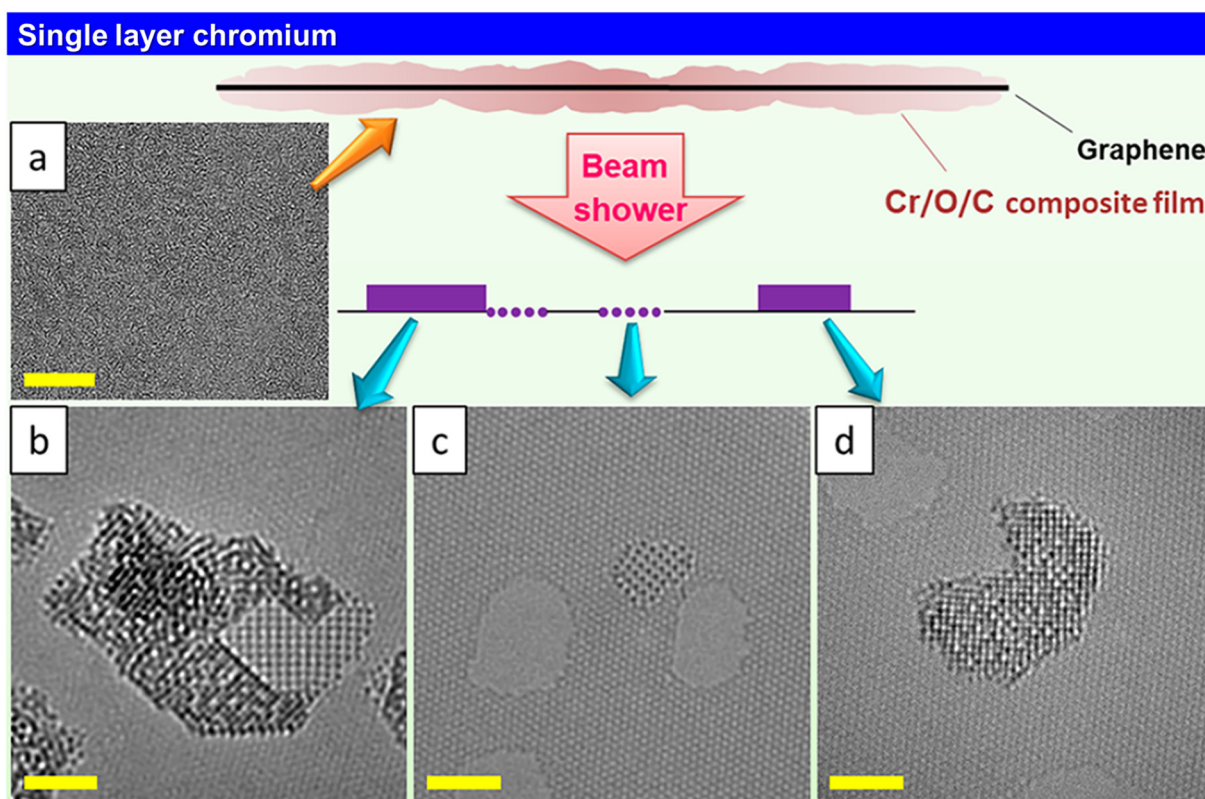
**Fig. 4** Schematics for synthesis of Cr membrane via electron beam irradiation. **(a)** TEM micrograph showing amorphous Cr, O, and C composite film on graphene prior to irradiation. **(b)** Partial chromium oxide NP with a 2D Cr single-atom-thick membrane. **(c)** Crystalline single-atom thick Cr membrane with square lattice in a graphene pore. **(d)** Chromium oxide NP over graphene. Scale bars are 10 nm in (a) and 2 nm in (b − d). Reprinted with permission from Ref. (Ta et al., 2020) Nano Lett. 2020, 20, 6, 4354–4361. Copyright [2020] American Chemical Society.

Recently, free-standing single-atom-thick crystalline 2D chromium membranes suspended in graphene pores were formed *in situ* via electron beam irradiation (Fig. 4) (Ta et al., 2020); that reduced CrO to Cr *in situ* using low-voltage (80 kV) spherical aberration-corrected transmission microscopy (LVACTEM). These Cr membranes exhibiting antiferromagnetic ground states are highly attractive for future spintronic applications and further consolidate the existence of a new class of elemental 2D metals. The lattice constant for the Cr membrane is less than that of the bulk Cr of 2.88–2.91 Å. To the best of our knowledge, so far, this is the first and only report regarding isolation of monolayer Cr.

## 7. Preparation methodologies

The properties and applications of 2D materials strongly depend up on their crystal structures and morphologies. Therefore, the synthesis and design of 2D materials are crucial to study their potential applications further. Various synthesis strategies such as top-down exfoliation, chemical vapor deposition (CVD), and thermal decomposition have been developed for their synthesis (Dong et al., 2018; Zhou et al., 2018; Xiao et al., 2018). The size, shape, and uniformity of 2D materials can be tuned to a certain extent by reforming experimental conditions such as concentrations, chemical reagents, and temperature.

Transition metal chalcogenides of Mo and W had been the subject of intensive research. Because Cr belongs to the same group of these elements, there is a dire need to study Cr-based materials to put their fascinating properties into potential applications. However, as the 3d orbital of Cr atom contains no radial node and thus its electrons are closer to the nucleus, it makes Cr different as well as a bit difficult from its group members. For Cr based compounds, the lower oxidation states of + 3 and + 2 are stable. On the contrary, owing to the presence of radial nodes in 4d and higher d orbitals, the higher oxidation states of Mo and W are more stable. Thus, the stability of Mo- and W-based compounds is different from those of Cr-based compounds. Consequently, the synthesis strategies that generally work for Mo and W, may not necessarily perform equally well for the synthesis of Cr compounds. Thus, the synthesis methods for fabricating Cr-based 2D materials require special attention and tailoring. The different methods for synthesizing Cr-based 2D compounds are summarized below.

### 7.1. Chemical vapor deposition (CVD)

CVD has distinct advantages such as high yield, large surface area, and large crystal domains of the product over other synthetic strategies (Dong et al., 2018). CVD is a commonly employed bottom-up synthesis approach for fabricating 2D

layered materials, most of which are van der Waal materials. Non-van der Waal materials are non-layered and preferably form 3D bonding, which makes their ultra-thin 2D fabrication difficult through conventional CVD growth. This limitation has been overcome using chemically inert and smooth substrates. Epitaxial growth has shown great success in growing 2D non-layered, non-van der Waal materials using the facile CVD synthesis. Unlike conventional epitaxies, such as molecular beam epitaxy and metal organic CVD, van der Waal epitaxy does not require a lattice match between the growing layer and the substrates. The lattice mismatch can act as a buffer against thermal stress in addition to facilitating the migration of the reaction precursors, resulting in high anisotropic growth with relatively high crystal quality, large lateral sizes, and defect-free crystals (Dong et al., 2018; Zhou et al., 2018). Mica, $MoS_2$, graphene, and h-BN are the examples of commonly used substrates for van der Waal epitaxy substrates because they are atomically smooth and have chemically inert surfaces (Dong et al., 2018).

In general, the CVD growth of Cr-based 2D materials (Fig. 5a) involves the use of a metal precursor either in the form of Cr powder or its halides/oxides that are further reacted with S, Se, or Te for chalcogenization (Habib et al., 2019; Zhou et al., 2019;29(3):1805880.; Li et al., 1999; Ishibashi et al., 1979; Aguilera et al., 2013; Bullen and Garrett, 2002). The crucial parameter in the CVD growth of 2D non-van der Waal materials is to effectively control the concentration

of the precursor to prevent the formation of their thermodynamically more stable 3D analogues (Zhou et al., 2019;29 (3):1805880.). Therefore, space-confined strategy that accelerates the horizontal rather than vertical growth of samples is generally adopted in addition to the use of van der Waal epitaxy substrates (Utama et al., 2013; Huang et al., 2017). Moreover, the Cr-based 2D non Vander Waal materials can be grown using salt-assisted CVD synthesis (Chu et al., 2019; Zhang et al., 2019). This involves mixing of a metal precursor and salt forms a molten solution that generates intermediate products, thereby increasing the vapor pressure by decreasing the melting point of the reactant (Chu et al., 2019; Han et al., 2019). In addition, the salt can act as a gaseous catalyst that increases the growth rate by decreasing the energy barrier (Zhang et al., 2019). Currently, CVD is the most successful technique for depositing $CrO_2$ thin films that has been used by various authors (Cho, 2003; Sousa et al., 2006; Li et al., 1999; Ishibashi et al., 1979; Aguilera et al., 2013; Bullen and Garrett, 2002),with minor modifications since it was first reported by Isibashi et al (Zhang et al., 2015; Ivanov et al., 2001; Ishibashi et al., 1979; Ishibashi et al., 1978).(See Fig. 6).

In addition to these strategies, another commonly used method involves the use of a gas-phase precursor metallographic limited dissolution technique that enables the synthesis of several Cr-based materials including telluride, selenide, and sulfide by CVD (Shivayogimath et al., 2019). Using this method, few-atom-thick binary compounds can be fabricated
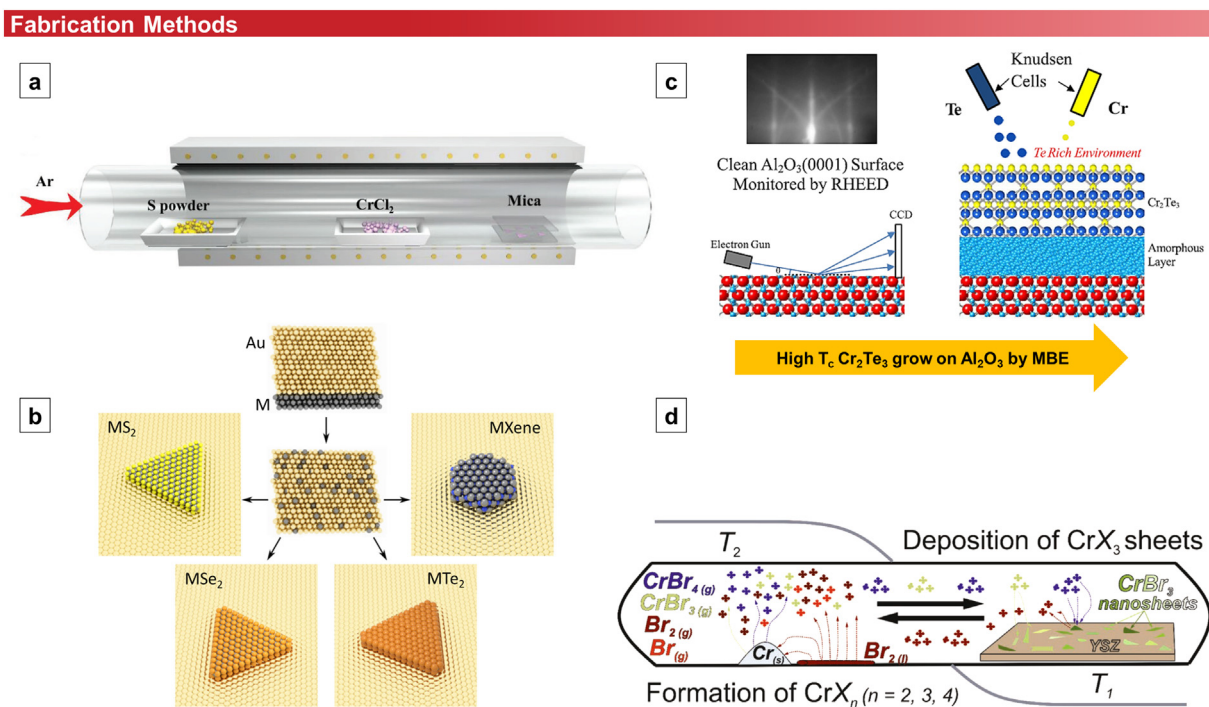


**Fig. 5** Different methods for fabricating the 2D Cr-based materials. **(a)** Schematic for CVD synthesis of ultrathin $Cr_2S_3$ flakes on two stacked mica sheets with $CrCl_2$ and S as the co-evaporation sources. Reproduced with permission from Ref. (Zhou et al., 2019;29 (3):1805880.). Copyright 2018, John Wiley and Sons. **(b)** A general approach for synthesizing thin layers of 2D binary compounds. Reproduced with permission from Ref. (Shivayogimath et al., 2019) Creative Commons CC BY, Springer Nature **(c)** Schematics of high-Tc $Cr_2Te_3$ thin films grown on $Al_2O_3$ via molecular beam epitaxy. Reprinted (adapted) with permission from Ref. (Li et al., 2019) [ACS Appl. Nano Mater. 2019, 2, 11, 6809–6817], copyright [2019] American Chemical Society. **(d)** Scheme for the one-step synthesis and vapor transport of $CrX_3$ (X = Br, I) micro- and nanosheets. Reproduced with permission from Ref. (Grönke et al., 2019). Creative Common License, John Wiley and Sons.
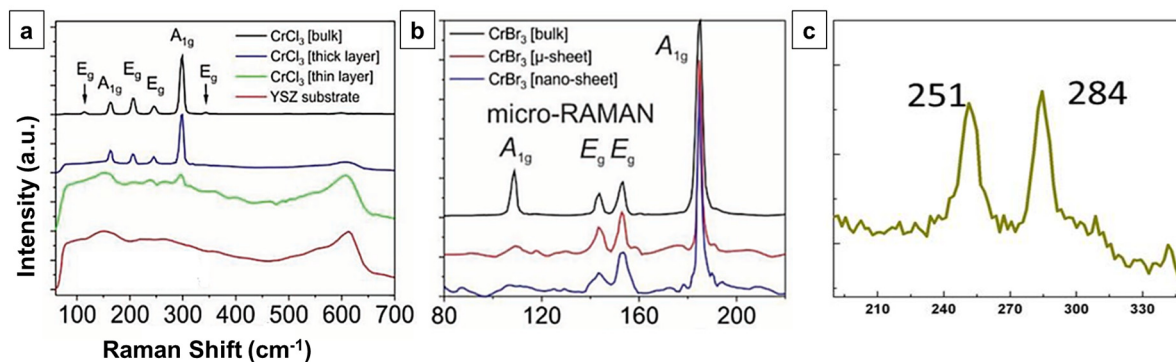
## Raman spectra



**Fig. 6** **(a)** Micro-Raman measurement of bulk $CrCl_3$ (black), $CrCl_3$ nanosheets (thick layer, blue), $CrCl_3$ nanosheets (thin layer, green), and of the pure YSZ substrate (red). **(b)** Micro-Raman measurement of bulk $CrBr_3$ (black), $CrBr_3$ microsheet (red), and a $CrBr_3$ nanosheet (blue). Reproduced with permission from Ref. (Grönke et al., 2019). Creative Common License, Jhon Wiley and Sons **(c)** Typical Raman spectrum of CrSe on $SiO_2$/Si. Reproduced with permission from Ref. (Zhang et al., 2019). Copyright 2019, John Wiley and Sons.

by varying the choice of X (= S, Se, Te) and metal, and different compounds can be obtained on the same growth substrate. (Fig. 5b).

### 7.2. Metal-organic CVD

Metal-organic CVD is the most promising techniques for thin film deposition as evinced by wafer-scale films (Eichfeld et al., 2015; Kang et al., 2015). For the growth of crystalline monolayer TMDs, powder precursors have been commonly used owing to their high reactivity at elevated temperatures and low costs. However, in CVD system, there is lack of control over the powder precursor supply. This limitation can be overcome using metal–organic CVD as it offers controlled precursor flowrates and therefore the growth time can be extended to hours (Och et al., 2021). In general, the metal–organic CVD precursors are required to have high reactivity, high volatility, stability and preferably low toxicity with a key requirement of less carbon content since its leads to accumulation of carbonaceous species on the substrate/product interface besides the product surface.

Among the different precursors used for the synthesis of $CrX_2$ using metal–organic CVD, chromium carbonyl precursor $(Cr(CO)_6)$ has a higher volatility rate. Moreover, pyrolysis of chromium carbonyl increase below 500 °C that facilitates films growth on temperature-sensitive substrates as compared to other commercially available complex organo-chromium precursors (Wei and Lo, 1998). For instance, with use of chromium carbonyl, the highest growth rate of $Cr_2O_3$ with negligible carbon contamination can be achieved at 500 °C precursors (Carta et al., 2005). Therefore, the use of chromium carbonyl precursors is generally preferred for MOCVD growth of $CrX_2$. Additionally, alkali metals salts are becoming popular precursors owing to increased domain size. Nevertheless, these too cause higher contamination of Na and epitaxy loss in the synthesized films (Kang et al., 2015). In MOCVD, the precursor purity significantly affect the quality of the film produced and difference of 99% and 99.99% becomes significant (Eichfeld et al., 2015). And thus makes MOCVD more expensive.

### 7.3. Physical vapor deposition (PVD)

Physical vapor deposition (PVD) techniques such as pulsed laser deposition (PLD) and molecular beam epitaxy (MBE) are commonly used for *in situ* fabrication of multilayer films and for developing high-quality interfaces (Heinig et al., 2007). Various Cr-based materials can be synthesized using these techniques. For instance, thin films of chromium sesquioxide $(Cr_2O_3)$ on Si have been prepared through pulsed laser deposition (PLD) (Tabbal et al., 2006). In addition, several groups have fabricated $CrO_2$ films on $TiO_2$ (Kang et al., 2015), Si (Constantin et al., 2004), Si (Kang et al., 2015), $Al_2O_3$ (0001), and $LaAlO_3$ (Kang et al., 2015) via MBE (Ingle et al., 2001) and PLD synthesis (Shima et al., 2002; Stanoi et al., 2005). Apart from chromium oxides, single-phased chromium oxynitride [Cr(Nx,Oy)] films on Si (Kang et al., 2015) substrates have also been synthesized using the PLD technique. The films structurally resembled CrN; however, the N atoms were partially substituted by oxygen. When different pressures of nitrogen were used in the presence of residual oxygen, it was established that a relatively smooth film surface was obtained when low pressure of nitrogen was used (Suzuki et al., 2002).

Similarly, thin films of CrN have been grown on MgO (0 0 1) substrates using radio-frequency N plasma-assisted MBE (Alam et al., 2017; Constantin et al., 2004). In addition, thin films of $Cr_2Te_3$ and $Cr_2Se_3$ had been deposited on Si and $Al_2O_3$ substrates using MBE (Fig. 5c) (Roy et al., 2020; Roy et al., 2015; Li et al., 2019; Pramanik et al., 2017). Additionally, single layer $CrI_3$ and ternary system of $Cr_2Ge_2Te_6$ has been prepared using MBE (Li et al., 2020; Mogi et al., 2018).

### 7.4. Chemical vapor transport (CVT)

CVT is a method for conducting heterogeneous reactions between a reactive gas phase and a condensed phase and it makes use of elevated temperature and temperature gradients (Lenz and Gruehn, 1997; Binnewies et al., 2013). The advantage of CVT is that it requires no additional carrier gas. The

use of CVT for the preparation of the Cr-based 2D materials has only recently emerged with reports regarding $CrPS_4$ and $CrX_3$ (X = Cl, Br, or I) synthesis (Lee et al.2018,; Grönke et al., 2019; De Siena et al., 2020), $CrX_3$ (X = Cl, Br, or I) micro- and nanocrystals have been directly deposited on a yttria-stabilized zirconia ($ZrO_2$:$Y_2O_3$) substrate in an endothermic process in two-zone furnaces conducted in quartz ampoules (Fig. 5d) (Grönke et al., 2019). Similarly; single-crystal $CrPS_4$ has been grown using Cr, P, and S precursor powders (Lee et al., 2018).

### 7.5. Atomic layer deposition

Atomic layer deposition (ALD) is a technique that uses gaseous precursors to grow desired films through chemical surface reactions(Leskelä et al., 2014). So far, ALD studies have focused on transition metal dichalcogenides and is a very active and rapidly growing field of research(Mattinen, 2020). For chromium based two-dimensional compounds the use of ALD is not very common. To the best of our knowledge, only $CrO_x$ films are commonly deposited using ALD method(Tarre et al., 2008; Jõgiaas et al., 2022; Daresibi et al., 2022). The atomic layer deposition method was used to synthesize $CrO_x$/$SiO_2$ catalysts for oxidation of propane to propylene using $CO_2$. The ALD synthesis method resulted in the higher dispersion of chromium oxide particles and higher specific reaction rates(Daresibi et al., 2022) when compare to CVD method of synthesis.

### 7.6. Mechanical exfoliation

Mechanical cleavage or the Scotch-tape method is the earliest, easiest, cheapest, and the most commonly used technique for producing mono-or few-layered 2D materials from their bulk counterparts (Samadi et al., 2018). This technique provides high-quality crystalline products with almost no or negligible defects. Besides, the degree of contamination in the product is relatively low as the process does not use chemicals (Zavabeti et al., 2020). Therefore, most of the basic physics and devices on 2D materials rely largely on this method (Choi et al., 2017).

Theoretically, the method can isolate single-layer 2D materials from any crystal with an atomic layered structure yet the method has some practical limitations. For instance, crystals that have ionic bond characteristics or more polar covalent bonds have strong interlayer coupling; therefore, peeling off their single layer from the corresponding natural crystal is difficult. In addition, the shape, size, and thickness of the nanosheets fabricated using this method exhibit random domain sizes and thicknesses and lack repeatability (Zavabeti et al., 2020). Moreover, the repeated transfer process is not scalable for practical purposes (Duan et al., 2015).

## 8. Structural characterization

After describing the different methods for the 2D chromium-based materials growth, the next step is to identify pathways for the reliable characterization technique required to determine the number of layers of these 2D materials. We review some of the primary techniques used to characterize the structure of Cr-based 2D materials.

### 8.1. Raman spectroscopy

Raman spectroscopy is a non-destructive characterization tool used to obtain information about the lattice vibrations of 2D crystals. For 2D materials, Raman spectroscopy is a basic tool for extracting information about its layer number. Starting with chromium halides $CrX_2$ (X = Cl, Br, I); micro-Raman study of bulk $CrCl_3$ shows four Eg (at 116.2, 208.6, 247.0, and 345.6 $cm^{-1}$) and two A1g (at 166.2 and 298 $cm^{-1}$) vibration modes (Kazim et al., 2020). As the layer number decreases (nanoscale), the peak intensity of the Raman vibrations decreases, and the two peaks lying at the extreme left and right (at 116.2 and 345.6 $cm^{-1}$) are the first to disappear from the Raman spectrum. In thinner or bilayers, the underlying substrate significantly influences the obtained results, and the only identifiable dominant peak is at 298 $cm^{-1}$. While for $CrBr_3$, there are four Raman active modes (two Eg at 152.5 and 142 $cm^{-1}$ and two A1g at 183.5 and 107 $cm^{-1}$ respectively) (Borghesi et al., 1984). For the micro- and nanosheets of $CrBr_3$, the intensity of the A1g peak at approximately 108 $cm^{-1}$ significantly decreased as compared to those of the bulk samples. $CrI_3$ nanosheets have extremely strong oxygen sensitivity under ambient conditions, which hinders a comprehensive study of these via micro-Raman (Grönke et al., 2019). Whereas for bulk $CrI_3$, the Raman spectrum constitutes only one lattice vibration of the Ag type at 110 $cm^{-1}$. For the nano- and micro-layered $CrI_3$, the total intensity of the acquired Raman peaks of were fairly decreased and broadened (Grönke et al., 2019). In some studies, the unpolarized Raman spectrum of bulk $CrI_3$ crystals has been reported to display a series of peaks at frequencies of 77.1, 100–110, 128.4, 231.7, and a weak, broad excitation at 253.2 $cm^{-1}$ (Shcherbakov et al., 2018).

For Cr chalcogenides, the Raman spectra of the polycrystalline $CrO_2$ films grown on Ti substrates are characterized by the presence of three prominent bands centered at $455 \pm 5$[1], $565 \pm 5$, and $683 \pm 5$ $cm^{-1}$ attributed to the vibrational modes Eg, $A_1g$, and $B_2g$ of the rutile substrate. Moreover, the orientation of the rutile single crystal with respect to the incident light determines the number of detected bands when examined via Raman spectroscopy. When light imping normally on the rutile (0 0 1) face, all three peaks are allowed. However, the $B_2g$ mode would be forbidden when the rutile (Alam et al., 2017) and (Kang et al., 2015) faces were examined (Aguilera et al., 2013). In addition, the type of substrate used to grow $CrO_2$ affects the number of Raman allowed modes. For instance, for $CrO_2$ grown on $Al_2O_3$ (0001), B1g (149 $cm^{-1}$) was active (Stanoi et al., 2005). Pristine $Cr_2O_3$ ultra-thin films exhibit a signature peak at 551 $cm^{-1}$ attributed to the A1g vibration mode (red shifted from its bulk value of 554 $cm^{-1}$). In addition, Eg modes were observed at 300, 350, 520, and 620 $cm^{-1}$ (Dutta et al., 2017).

The different stoichiometries of chromium sulfides have similar yet distinguishable Raman features. For all chromium sulfides, the Raman spectra constitute four primary peaks at ca. 175, ca. 253, ca. 285, and ca. 364.0 $cm^{-1}$ (with $\pm$ 10) (Habib et al., 2019; Zhou et al., 2019;29(3):1805880.; Cui et al., 2020;32(4):1905896.). The peak at 253 $cm^{-1}$ corresponds to the in-plane Eg mode, whereas the other three peaks correspond with the out-of-plane Ag modes. In spite of that, the difference in the strength of the covalent bond between Cr and S

atoms affects the Raman shift. For non-layered rhombohedral $Cr_2S_3$, an increase in layer thickness results in a red-shift of the four peaks, which is mainly attributed to the change in the covalent bond strength between S and Cr atoms owing to the stacking effect (Zhou et al., 2019;29(3):1805880.; Cui et al., 2020;32(4):1905896.). For CrSe, the Raman spectra exhibited only two peaks at 251 and 284 cm$^{-1}$. Additionally, the Raman peaks become intense and show blue shifts with decreasing thickness (Zhang et al., 2019).

For chromium ternary compounds such as CrSiTe$_3$ has three Raman active modes of Eg, Ag$^2$, and Ag$^1$ symmetry that appear at 101, 125, and 142 cm$^{-1}$, respectively, corresponding to the in-plane and out-of-plane vibrations of Te atoms (Lin et al., 2016). The Raman spectra of the freshly cleaved $Cr_2Ge_2Te_6$ sample exhibit seven modes centered at 78.6, 85.3, 110.8, 136.3, 212.9, 233.9, and 293.8 cm$^{-1}$ at 270 K at room temperature (Tian et al., 2016).

### 8.2. X-ray photoelectron spectroscopy (XPS)

X-ray photoelectron spectroscopy (XPS) is another commonly used technique for confirming the bonding state and elemental composition of 2D materials. The different oxidation states ($Cr^{+3}$, $Cr^{+4}$, and $Cr^{+6}$) can be differentiated from the XPS profiles. For $Cr^{+3}$, the Cr 2p3/2 and Cr 2p1/2 peaks were located at 578.08 ($\pm 5$) and 587.8 ($\pm 5$) eV, respectively. Moreover, a satellite peak was observed at 10.5 ($\pm 5$) eV. In case of $Cr^{+6}$, the Cr 2p3/2 and Cr 2p1/2 peaks were located at 589.3 ($\pm 2$) and 580.2 ($\pm 2$) eV respectively with no satellite peaks. Moreover, the full width half maxima of the peaks decreased

(Okamoto et al., 1976). For $Cr^{+4}$, the fitting curves of Cr 2p state were located at 576.3 $\pm$ 0.3 and 586.4 eV, corresponding to Cr 2p3/2 and Cr 2p1/2 peaks, respectively (Habib et al., 2019; Zhou et al., 2019;29(3):1805880.; Cui et al., 2020;32(4):1905896.; Zhang et al., 2019). For the unoxidized, $Cr^0$ state, the Cr 2p3/2 and Cr 2p1/2 peaks were located at 574.5 and 583.6 eV, respectively (Okamoto et al., 1976). For $Cr^{+4}$; the XPS absorption values lie in the lower region, followed by $Cr^{+3}$ and then $Cr^{+6}$ (Ingle et al., 2001). The high XPS absorption values for $Cr^{+3}$ than $Cr^{+4}$ are attributed to the extra stability associated with the half-filled 3d orbital in $Cr^{+3}$.

For anionic part in $Cr_2S_3$, the S 2p3/2 and S 2p1/2 peaks were located at 160.9 and 162.0 eV, respectively (Habib et al., 2019; Zhou et al., 2019;29(3):1805880.; Cui et al., 2020;32(4):1905896.). For CrS, the two peaks were reported to show a shift of 2.0 and 1.4 eV, respectively. Besides, another peak was observed at 163.8 eV, indicating the S-rich characteristic (Habib et al., 2019). In case of CrSe, the peaks of Se were observed at 55 and 53 eV, corresponding to the 2p1/2 and 2p3/2 states of Se, respectively (Zhang et al., 2019). For Te, the XPS absorption region overlaps with Cr2p. To differentiate between Cr and Te, the region from 550 to 600 eV should be scanned to acquire both Te 3d5/2 and Te 3d3/2 components that appear at 573 and 583.1 eV, respectively (Rodríguez-de Marcos et al., 2020).

### 8.3. X-ray diffraction spectroscopy (XRD)

X-ray diffraction spectroscopy (XRD) is a technique primarily employed to identify and study crystal structures (Zhang et al.,
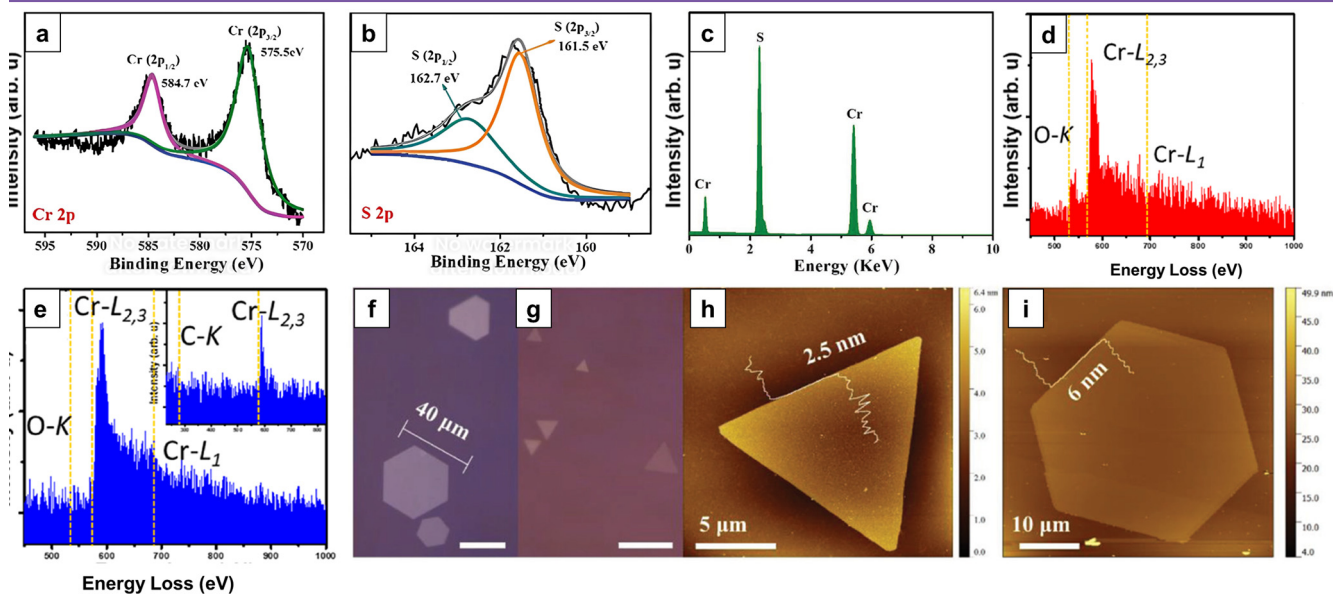


**Fig. 7** **(a)** XPS characterization of Cr 2p and **(b)** S 2p of the as-grown $Cr_2S_3$. **(c)** EDX spectrum of the $Cr_2S_3$ nanoflake. Reproduced with permission from Ref. (Zhou et al., 2019;29(3):1805880.). Copyright 2018, John Wiley and Sons. **(d, e)** Local electron energy loss spectroscopy (EELS) profiles of CrO NP (red spectrum) and 2D Cr membrane (blue spectrum). Reproduced with permission from Reprinted with permission from Ref. (Ta et al., 2020) [Nano Lett. 2020, 20, 6, 4354–4361]. Copyright [2020] American Chemical Society. **(f, g)** Optical images of the as-synthesized $Cr_2S_3$ flakes. Scale bar: 20 μm. **(h, i)** AFM images and height profiles of triangular and hexagonal samples, respectively. Reproduced with permission from Ref. (Zhou et al., 2019;29(3):1805880.). Copyright 2018, John Wiley and Sons.

2019). For Cr-based 2D materials, the XRD intensity profile is used to determine the layer thickness (Sousa et al., 2007). Moreover, XRD characterization provides key information about the deposition orientation of the films based on the substrate and the different phases present (Cho, 2003; Rabe et al., 2001; Habib et al., 2019; Gharavi et al., 2018;51(35):355302.; Chen, 2003).

### 8.4. Atomic force microscopy

Atomic force microscopy (AFM) is a powerful imaging technique for almost any type of surface including two dimensional materials. Topographic images often do not correlate to material properties. For this purpose, AFM is used to study different properties of materials such as magnetic and electrical forces, resistance, conductivity, friction, capacitance, surface potential etc (Liu et al., 2014). For chromium-based compounds, the technique has been widely used to investigate the height profiles (Chu et al., 2019; Zhou et al., 2019;29 (3):1805880.; Zhang et al., 2019; Lee et al., 2018; Grönke et al., 2019) as shown in Fig. 7 (h, i).

### 8.5. Electron spectroscopies

SEM is a characterization technique primarily used for studying the topographical information and for microstructural analyses such as grain boundaries, patches, grain shape, and number of layers (Heinig et al., 2007). In addition, high-resolution TEM (HRTEM) is used to identify the crystalline structure with atomic resolution as commonly used for characterization of other 2D materials. Additionally, it is used to assess the quality and thickness of the crystal structure as well as the lattice plane spacing (Zhang et al., 2019). Figs. 8 and 9 show a library of SEM and TEM micrographs of the different Cr-based 2D materials, respectively.(See Fig. 10).

Supplement to the above-mentioned techniques, energy-dispersive spectroscopy (EDS) has been commonly used for the elemental quantification of Cr-based compounds (Zhang et al., 2019; Li et al., 2019; Mogi et al., 2018; Grönke et al., 2019), besides electron energy loss spectroscopy (EELS) that has been used to characterize a single-layer Cr produced from the reduction of CrO nanoparticles. As shown in Fig. 7e, for monolayer chromium membrane, only Cr $L_{2,3}$ edges were observed in EELS.

## 9. Applications

### 9.1. Spintronics and Magnonics

The recent surge in information and the ever-reducing size of electronic devices has created demand for new high-density data storage solutions that combine longer retention times
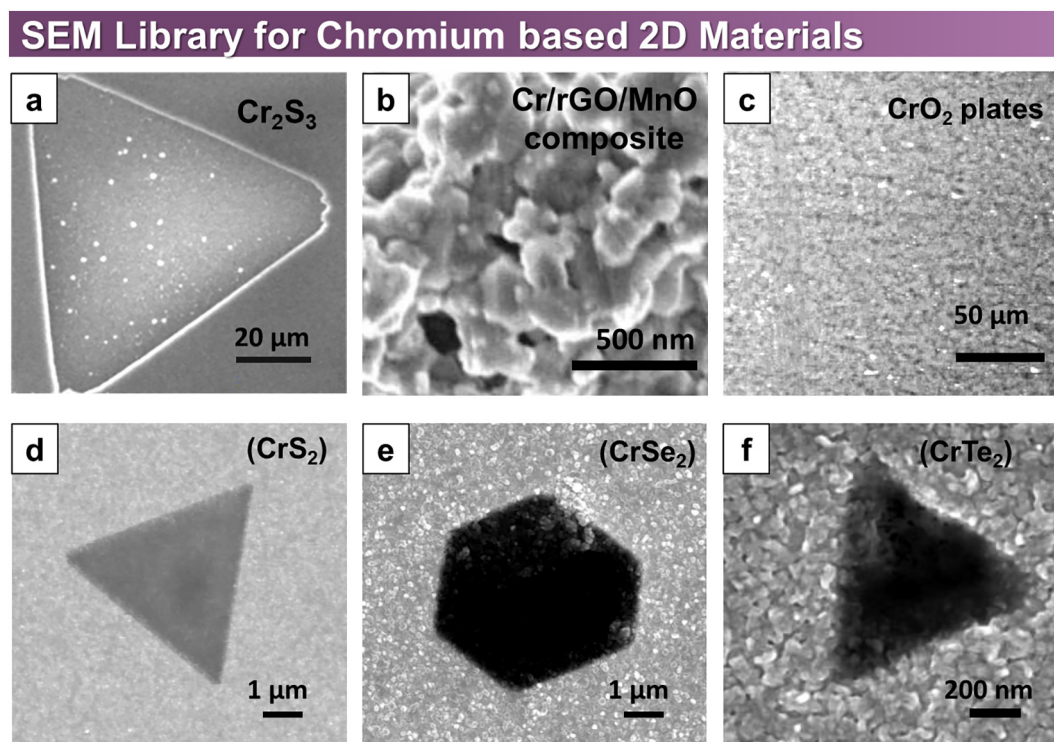


**Fig. 8** Library of scanning electron microscopy (SEM) images of 2D Cr-based compounds. **(a)** SEM image of $Cr_2S_3$ nanosheet. ''Reprinted (adapted) with permission from Ref. (Chu et al., 2019) [Nano Lett. 2019, 19, 3, 2154–2161]. Copyright [2019] American Chemical Society.'' **(b)** SEM image of Cr/rGO nanocomposite with MnO. Reproduced with permission from Ref. (Sun et al., 2020) **(c)** SEM images of a $CrO_2$ film. Reproduced with permission from Ref. (Stanoi et al., 2005). ''Reprinted from Publication Chromium oxides thin films prepared and coated *in situ* with gold by pulsed laser deposition, 118, D. Stanoi, G. Socol, C. Crigorescu, F. Guinneton, O. Monnereau,L. Tortet, T. Zhang, I.N. Mihailescu Copyright (2005), with permission from Elsevier **(d-f)** SEM images of different Cr chalcogenides. Reproduced with permission from Ref. (Shivayogimath et al., 2019). Creative Commons CC BY, Springer Nature.
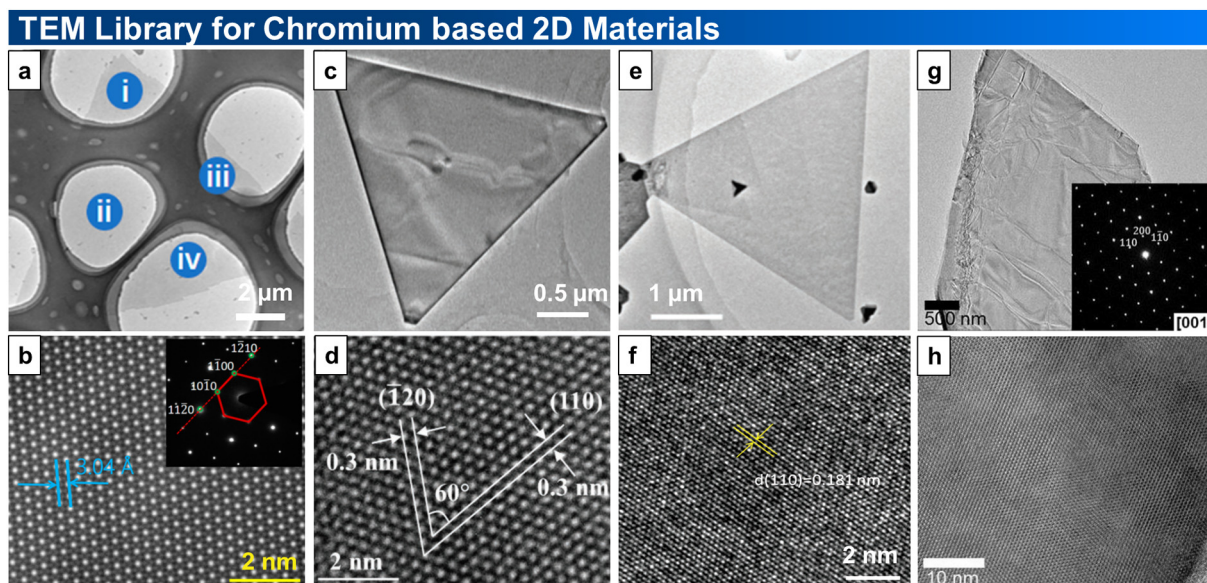
**TEM Library for Chromium based 2D Materials**



**Fig. 9** TEM characterization of Cr-based 2D materials. **(a)** Low-magnification image of a single-crystal $Cr_2S_3$ domain transferred on a copper grid. **(b)** HAADF-STEM image of the inner area of the $Cr_2S_3$ nanosheet. ''Reprinted (adapted) with permission from Ref. (Chu et al., 2019) [Nano Lett. 2019, 19, 3, 2154–2161]. Copyright [2019] American Chemical Society.'' **(c)** Low-magnification TEM image. **(d)** HRTEM image of a $Cr_2S_3$ nanoflake. Reproduced with permission from Ref. (Zhou et al., 2019;29(3):1805880.). Copyright 2018, John Wiley and Sons. **(e)** TEM image of a triangular CrSe flake. **(f)** HRTEM image of a CrSe crystal. Reproduced with permission from Ref. (Zhang et al., 2019). Copyright 2019, John Wiley and Sons **(g)** Low-magnification TEM image showing a wide area of single crystalline $CrPS_4$. **(h)** HRTEM image. Reproduced with permission from Ref. (Lee et al., (CrPS 4). 2018). Creative Commons CC BY license.

and fast responses. High-efficiency hard drive read heads use magnetic phenomena such as giant magnetoresistance (GMR) and tunnel magnetoresistance (TMR) effects, which have fueled the big data and cloud era revolution (Och et al., 2021). Spintronic technology has been applied to ultra-low power memory circuits such as magnetic random access memories (MRAMs) and they are progressively being integrated into CMOS-based devices. 2D ferromagnetic (FM) materials can lead to a complete 2D magnetic tunnel junction. Moreover, 2D ferromagnets are the perfect source of fully polarized spin that naturally offers infinite TMR for a 2D magnetic tunnel junction (MTJ), which is a long-awaited goal in the field of spintronics. Although the Mermin Wagner Hohenberg (MWH) theorem predicted spontaneous magnetization in 2D materials, it was only very recently discovered in $CrI_3$, $CrGeTe_3$, and $Fe_3GeTe_2$ (Gong et al., 2017; Huang et al., 2017; Tian et al., 2016; Wang et al., 2018; Deiseroth et al., 2006).

$CrI_3$ is a layered AFM insulator that can act as a spin-filtering barrier for 2D MTJs. It reveals powerful spin-filtering properties in devices fabricated by sandwiching $CrI_3$ between graphene electrodes (Song et al., 2018; Klein et al., 2018; Kim et al., 2018). These MTJs result from magnon-mediated tunneling, in contrast to the conventional electron or phonon-mediated tunneling (Klein et al., 2018; Ghazaryan et al., 2018). The internal $CrI_3$ interlayer exhibited an applied magnetic field-induced transition from AFM to FM in a way similar to giant magnetoresistance behavior. In the AFM state, every $CrI_3$ layer filters out an opposite spin direction, thus increasing the resistance of the tunnel barrier. Conversely, with an applied magnetic field, all the layers would align, allowing a preferential spin direction to pass through and thus reducing

the overall resistance. Owing to the high spin-filtering efficiency, large TMR in the million-percent range was established (Kim et al., 2018; Song et al., 2019). Moreover, the TMR can be modulated using voltage, sample thickness, and biasing conditions, thus creating the possibility of voltage-controlled van der Waal spintronic devices (Song et al., 2019; Kim et al., 2019). This effective spin-filtering effect and electrically switchable magnetic order of $CrI_3$ provides a new operating principle for spin-tunnel field-effect transistors (Jiang et al., 2019).

Using density functional theory $CrS_2$ has been discovered to possess the most diverse electronic and magnetic properties: antiferromagnetic (AFM) metallic 1 T phase, non-magnetic (NM) semiconductor 2H phase, and ferromagnetic (FM) semiconductor 1 T′ phase with a Curie temperature of $\sim$ 1000 K. The study found that a tensile or compressive strain can turn 1 T′ $CrS_2$ into a spin-up or spin-down half-metal that has not been observed in other 2D materials before. This feature allows strain engineering in different regions of a $CrS_2$ nanosheet to readily switch and match spin conduction channels for spin current control (Chen et al., 2021). In addition, switching of the semiconducting van der Waals ferromagnet $CrGeTe_3$ through spin–orbit torque has been demonstrated at Ta interface, which has potential applications in logic applications and low-power memory (Ostwal et al., 2020). Moreover, Novel FM materials (e.g., $CrSiTe_3$ and $CrGeTe_3$) are promising ultrathin nanomaterials for potential spintronics applications (Lin et al., 2016; Wang et al., 2018).

Magnonics is a topical and rapidly developing branch of spintronics and magnetoelectronics that refer to the use of magnon-mediated spin currents for computing and information logic applications, the so called magnon-based spintronics
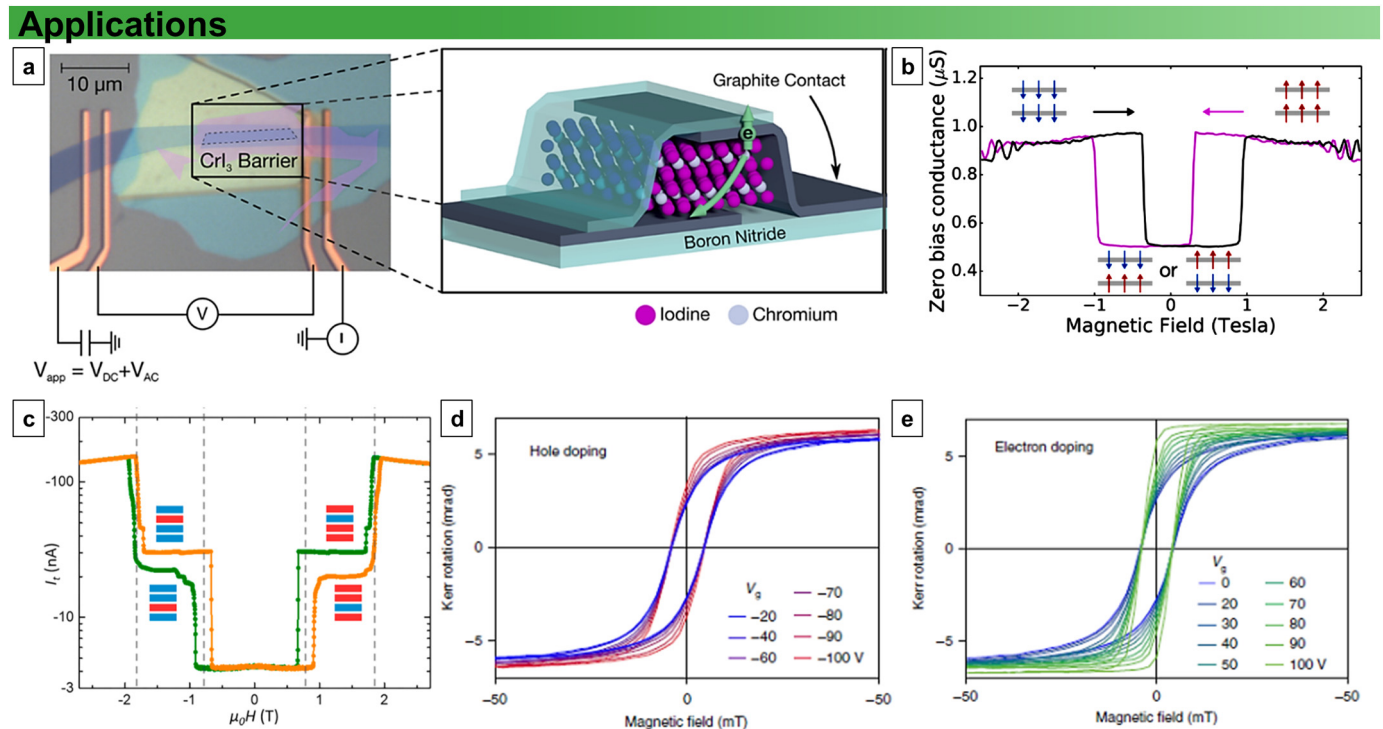
## Applications



**Fig. 10** **(a–b)** Optical image and schematic of a Gr/CrI₃/Gr MTJ and measured magnetoconductance vs. applied magnetic field. Adapted with permission from Ref. (Deiseroth et al., 2006) From [D. R. Klein et al., Science https://doi.org/10.1126/science.aar3617 (2018).] Reprinted with permission from AAAS. **(c)** Schematic of a four-layer CrI₃ sf-MTJ device including two monolayer graphene contacts as well as top and bottom gates. **(d)** Tunneling current (It) of the same device at representative bias and gate voltages (V = − 240 mV, Vtg = 0 V, and Vbg = 0 V). Reprinted (adapted) with permission from Ref. (Ghazaryan et al., 2018) [Nano Lett. 2019, 19, 2, 915–920]. Copyright [2019] American Chemical Society. **(e)** Normalized anomalous Hall resistance for three different Cr₂Ge₂Te₆ thicknesses. Reproduced with permission from Ref. (Chen et al., 2021). Copyright 2020 John Wiley and Sons.

(Nikitov et al., 2015). Here too Cr-based 2D FM materials have potential applications (Chumak et al., 2015). Recently, long-distance magnon transport was demonstrated in 3D antiferromagnetic Cr₂O₃ (Yuan et al., 2018). In addition, the discovery of intrinsic ferromagnetism in chromium-based 2D vdW crystals, for example CrI₃, Cr₂Ge₂Te₆, CrTe₂ has stimulated intense interest in magnetic order at the ultimate 2D limit and may promise exciting technological opportunities for magnetic sensing and information storage (Purbawati et al., 2020; Kuklin et al., 2020). Many of these 2D vdW magnets exhibit tunable magnetic properties depending on the number of atomic layers and the exact interlayer coupling mechanism. For example, exfoliated CrI₃ exhibits layer-number-dependent magnetic states resulting from interlayer antiferromagnetic (AFM) coupling, Cr₂Ge₂Te₆ display a monotonic increase in the Curie temperature with increasing thickness. In addition, R- and H-stacked CrBr₃ bilayers demonstrate antiferromagnetism and ferromagnetism, respectively (Li et al., 2021).

### 9.2. Synaptic devices

The way neural system process information provides a model that can be emulated to develop artificial multifunctional neuromorphic applications in addition to low energy consumption. However, this requires the development of synaptic devices with tunable weights. Owing to their unique chemical and physical properties as well as atomic thickness, different 2D materials provide a suitable platform for fabricating synaptic devices such as two-terminal memristors (Lee et al., 2018; Cao et al., 2021; Zhao et al., 2020), heterosynaptic devices (Yang et al., 2019), multiterminal synaptic networks (Sangwan et al., 2018; Tian et al., 2016), synaptic transistors (Han et al., 2019) and optoelectronic synaptic devices (Zhuge et al., 2019;13(9):1900082.).

Lee et al. reported an artificial synapse, with 2D-layered chromium thiophosphate (CrPS₄) sandwiched by Ag and Au electrodes that demonstrate multiple resistance states using a voltage bias smaller than 0.3 V in which weights were stored by controlling Ag or Cu filaments inside the CrPS₄ layer. They demonstrated that vertical capacitors could be promising inorganic synaptic devices that are compatible with next-generation neuromorphic technologies. Various functions, such as STP to LTP transition and synaptic plasticity, have been demonstrated in this device (Lee et al., 2018). The + 3 oxidation state of Cr in CrX₃ (X = Cl, Br, I) monolayers makes these 2D FM materials biocompatible. These 2D materials have been predicted to have potential applications in biomedicine, such as magnetically directed drug delivery, hyperthermia treatment of tumors, and magnetic labeling etc (Liu et al., 2016).

## 9.3. Fuel cells and batteries (ORR/OER/HER)

To date, Cr-based 2D materials lack practical demonstration for fuel cell and battery application. Nevertheless, first-principle calculations predict that the free energy for the Volmer reaction of 2H-CrS$_2$ monolayer with S vacancies is 0.07 eV, that is comparable with Pt-based catalyst. The S vacancy leads to defect states in the middle of electronic band-gap and the reduction of potential barrier between the S atom layer and the vacuum, which is conducive to improve HER performance (Sun et al., 2020). In addition, mesoporous CrN-reduced graphene oxide (rGO) nanocomposites with MnO have shown enhanced electrocatalytic ORR properties with superior performance to 20 wt% Pt/C (Khan et al., 2019). For batteries, Xi et al. introduce a cathode with Ru doping in Cr oxide for sodium-ion batteries that has an extended reversible discharge capacity of 156 mAh g$^{-1}$ (Xi et al., 2020). These studies indicate that the Cr-based 2D materials could be a serious option for the battery industry.

## 10. Challenges and drawbacks

A primary challenge associated with synthesis and fabrication of 2D ferromagnetic materials is their instability under ambient conditions. This is the reason why most of these materials need to be mechanically exfoliated from their bulk in precisely regulated environments, such as in glove box. Once isolated, these have relatively short lifetimes, low throughput, and limited control over the layer thickness (Gong et al., 2017; Huang et al., 2017) and therefore are extremely sensitive to the synthetic or post-synthetic processing conditions. As a resultant, the direct synthesis of these materials is much more difficult as compared to other 2D materials (Li et al., 2021). In addition to this, the inheritance of magnetism from their 3D bulk form to 2D in individual monolayers is not guaranteed a priori, and it depends on the magnetic anisotropy of the system. For instance, materials with isotropic exchange interactions can be magnetic in their 3D form, but thermal fluctuations strongly suppress the critical temperature as we reduce their thickness, until magnetism can eventually be destroyed at the 2D limit. This is the case for Cr GeTe$_3$, for which the critical temperature goes to zero as monolayer limit is approached (Gibertini et al., 2019). Among the major research challenge is to search for a suitable magnon transport channel material, which can propagate magnons over longer distances.

## 11. Conclusion and outlook

So far significant progress has been made in the field of Cr-based 2D materials. The bulk of this effort has focused on providing a concise overview on the Cr-based 2D materials. This review introduces the crystal structure, properties, synthesis strategies, structural characterization, and applications of the Cr-based 2D materials. Cr-based 2D materials with magnetic ordering have attracted significant interest in fundamental physics and the fabrication of novel devices. In this study, different strategies for synthesizing the Cr-based 2D materials have been discussed; however, each method has its own challenges. Nevertheless, 2D heterostructure magnets grown via CVD could contribute majorly to the emerging field of spintronics circuits. As the use of CVD has revolutionized the investigation of graphene, it is also expected for

the 2D Cr materials. Novel controllable synthetic strategies and the introduction of dopants into 2D Cr materials can significantly extend their application scope. Additionally, atomic layer deposition, as well as other nano-synthesis methods such as anion exchange mechanisms or sol gel mechanisms, should be thoroughly explored to produce chromium-based two-dimensional materials. Furthermore, characterization techniques such as atomic force microscopy (AFM), cyclic voltammetry, UV–visible spectroscopy, and impedance spectroscopy should be investigated to gain a comprehensive understanding of the structure and properties of chromium-based two-dimensional materials. Currently, our understanding of the fundamental properties and device fabrication of Cr-based 2D materials is still in its early stages. The isolation of single-layer chromium has opened up opportunities for customizing various Cr-based materials by introducing dopants into the chromium sheets, and a significant research breakthrough is expected in the field of magnetic materials. We believe that there is much more to be discovered in the field of energy production and batteries by delving deeper into the study of Cr-based 2D materials.

## Declaration of Competing Interest

The authors declare that they have no known competing financial interests or personal relationships that could have appeared to influence the work reported in this paper.

## Author Contributions

Maria Hasan carried out the literature survey and wrote the introduction and the different sub classes of the chromium based 2D materials, Huy Q. Ta did the literature survey and wrote the different preparation methodologies, Sami Ullah carried out the literature survey regarding the characterization techniques. Xiaoqin Yang carried out the literature survey relevant to the applications. Jingping Luo helped with getting the permissions for figures reproduction, Alicja Bachmatiuk participated in the sequence alignment, Thomas Gemming and Barbara Trzebicka helped in reviewing and editing, Azhar Mahmood and Mengqi Zeng helped in revising the manuscript and provided the key intellectual support, Lei Fu and Lijun Liu collected and edited the figures, Mark H. Rümmeli conceived the initial idea, supervised the team and provided funding. All authors read and approved the final manuscript.

## Additional Information

Correspondence and requests for materials should be addressed to Mark H. Rümmeli.

## References

Adachi Y, Izaki K, Koike K, Morita H, Kaneko T, Kimura H, et al. Electrical resistivity and magnetic property for Cr2Se3 and its Te-substitution system. 2007;310(2):1849-50

Aguilera, C., González, J., Borrás, A., Margineda, D., González, J., González-Elipe, A.R., et al, 2013. Preparation and characterization of CrO2 films by low pressure chemical vapor deposition from CrO3. Thin Solid Films 539, 1–11.

Alam, K., Disseler, S.M., Ratcliff, W.D., Borchers, J.A., Ponce-Pérez, R., Cocoletzi, G.H., et al, 2017. Structural and magnetic phase transitions in chromium nitride thin films grown by rf nitrogen plasma molecular beam epitaxy. Phys. Rev. B 96, (10) 104433.

Alegria L, Ji H, Yao N, Clarke J, Cava RJ, Petta JRJAPL. Large anomalous Hall effect in ferromagnetic insulator-topological insulator heterostructures. 2014;105(5):053512

Ares, P., Novoselov, K.S., 2021. Recent advances in graphene and other 2D materials. Nano Mater. Sci.

Audier M, Salaün M, Roussel H, Delyon Fo, Duneau MJCg, design. CrO2-to-Cr2O3 Transformation in a Three-Dimensional Interference Field of Ultraviolet Laser Light. 2010;10(4):1923-8

Baltz, V., Manchon, A., Tsoi, M., Moriyama, T., Ono, T., Tserkovnyak, Y., 2018. Antiferromagnetic spintronics. Rev. Mod. Phys. 90, (1) 015005.

Bao J-K, Liu J-Y, Ma C-W, Meng Z-H, Tang Z-T, Sun Y-L, et al. Superconductivity in quasi-one-dimensional K 2 Cr 3 As 3 with significant electron correlations. 2015;5(1):011013

Binnewies, M., Glaum, R., Schmidt, M., Schmidt, P., 2013. Chemical vapor transport reactions–a historical review. Z. Anorg. Allg. Chem. 639 (2), 219–229.

Blackman CS, Carmalt CJ, Manning TD, Parkin IP, Apostolico L, Molloy KCJAss. Low temperature deposition of crystalline chromium phosphide films using dual-source atmospheric pressure chemical vapour deposition. 2004;233(1-4):24-8

Borghesi, A., Guizzetti, G., Marabelli, F., Nosenzo, L., Reguzzoni, E., 1984. Far-infrared optical properties of CrCl3 and CrBr 3. Solid State Commun. 52 (4), 463–465.

Bullen, H.A., Garrett, S.J., 2002. Epitaxial growth of CrO2 thin films on TiO2 (110) surfaces. Chem. Mater. 14 (1), 243–248.

Cai T-Y, Li X, Wang F, Sheng J, Feng J, Gong C-DJapa. Emergent topological and half semimetallic Dirac fermions at oxide interfaces. 2013

Cao G, Meng P, Chen J, Liu H, Bian R, Zhu C, et al. 2D material based synaptic devices for neuromorphic computing. 2021;31 (4):2005443

Carta, G., Natali, M., Rossetto, G., Zanella, P., Salmaso, G., Restello, S., et al, 2005. A comparative study of Cr2O3 thin films obtained by MOCVD using three different precursors. Chem. Vap. Depos. 11 (8–9), 375–380.

Casto L, Clune A, Yokosuk M, Musfeldt J, Williams T, Zhuang H, et al. Strong spin-lattice coupling in CrSiTe3. 2015;3(4):041515

Chen, K., Deng, J., Yan, Y., Shi, Q., Chang, T., Ding, X., et al, 2021. Diverse electronic and magnetic properties of CrS2 enabling strain-controlled 2D lateral heterostructure spintronic devices. npj Comput. Mater. 7 (1), 1–9.

Chen X, Qi J, Shi DJPLA. Strain-engineering of magnetic coupling in two-dimensional magnetic semiconductor CrSiTe3: Competition of direct exchange interaction and superexchange interaction. 2015;379(1-2):60-3

Chen H-Y, Lu F-HJJoVS, Technology A: Vacuum S, Films. Phase transformation in chromium nitride films. 2003;21(3):695-700

Chhowalla, M., Shin, H.S., Eda, G., Li, L.J., Loh, K.P., Zhang, H., 2013. The chemistry of two-dimensional layered transition metal dichalcogenide nanosheets. Nat. Chem. 5 (4), 263–275.

Cho YN, DeSisto WJJCVD. Phase-Selective CVD of Chromium Oxides from Chromyl Chloride. 2003;9(3):121-4

Choi, W., Choudhary, N., Han, G.H., Park, J., Akinwande, D., Lee, Y.H., 2017. Recent development of two-dimensional transition metal dichalcogenides and their applications. Mater. Today 20 (3), 116–130.

Chu, J., Zhang, Y., Wen, Y., Qiao, R., Wu, C., He, P., et al, 2019. Sub-millimeter-Scale Growth of One-Unit-Cell-Thick Ferrimagnetic Cr2S3 Nanosheets. Nano Lett. 19 (3), 2154–2161.

Chua R, Zhou J, Yu X, Yu W, Gou J, Zhu R, et al. Room temperature ferromagnetism of monolayer chromium telluride with perpendicular magnetic anisotropy. 2021;33(42):2103360

Chumak, A.V., Vasyuchka, V.I., Serga, A.A., Hillebrands, B., 2015. Magnon spintronics. Nat. Phys. 11 (6), 453–461.

Constantin, C., Haider, M.B., Ingram, D., Smith, A.R., 2004. Metal/semiconductor phase transition in chromium nitride (001) grown by rf-plasma-assisted molecular-beam epitaxy. Appl. Phys. Lett. 85 (26), 6371–6373.

Cui F, Zhao X, Xu J, Tang B, Shang Q, Shi J, et al. Controlled growth and thickness-dependent conduction-type transition of 2D ferrimagnetic Cr2S3 semiconductors. 2020;32(4):1905896

Daresibi, F.G., Khodadadi, A.A., Mortazavi, Y., Huotari, S., Ritala, M., 2022. Highly dispersed atomic layer deposited CrOx on SiO2 catalyst with enhanced yield of propylene for CO2–mediated oxidative dehydrogenation of propane. Mol. Catal. 526, 112396.

De Siena, M.C., Creutz, S.E., Regan, A., Malinowski, P., Jiang, Q., Kluherz, K.T., et al, 2020. Two-dimensional van der Waals nanoplatelets with robust ferromagnetism. Nano Lett. 20 (3), 2100–2106.

Deiseroth HJ, Aleksandrov K, Reiner C, Kienle L, Kremer RK. Fe3GeTe2 and Ni3GeTe2–Two New Layered Transition-Metal Compounds: Crystal Structures, HRTEM Investigations, and Magnetic and Electrical Properties. Wiley Online Library; 2006

Dijkstra J, Weitering H, Van Bruggen C, Haas C, De Groot RJJoPCM. Band-structure calculations, and magnetic and transport properties of ferromagnetic chromium tellurides (CrTe, Cr3Te4, Cr2Te3). 1989;1(46):9141.

Dong, R., Zhang, T., Feng, X., 2018. Interface-assisted synthesis of 2D materials: trend and challenges. Chem. Rev. 118 (13), 6189–6235.

Duan, X., Wang, C., Pan, A., Yu, R., Duan, X., 2015. Two-dimensional transition metal dichalcogenides as atomically thin semiconductors: opportunities and challenges. Chem. Soc. Rev. 44 (24), 8859–8876.

Dutta, S., Pandey, A., Jain, K., 2017. Growth and characterization of ultrathin TiO2-Cr2O3 nanocomposite films. J. Alloy. Compd. 696, 376–381.

Eichfeld, S.M., Hossain, L., Lin, Y.-C., Piasecki, A.F., Kupp, B., Birdwell, A.G., et al, 2015. Highly scalable, atomically thin WSe2 grown via metal–organic chemical vapor deposition. ACS Nano 9 (2), 2080–2087.

Era H, Ide Y, Nino A, Kishitake KJS, Technology C. TEM study on chromium nitride coatings deposited by reactive sputter method. 2005;194(2-3):265-70

Fawcett, E., 1988. Spin-density-wave antiferromagnetism in chromium. Rev. Mod. Phys. 60 (1), 209.

Gharavi MA, Kerdsongpanya S, Schmidt S, Eriksson F, Nong N, Lu J, et al. Microstructure and thermoelectric properties of CrN and CrN/Cr2N thin films. 2018;51(35):355302

Gharavi MA, Greczynski G, Eriksson F, Lu J, Balke B, Fournier D, et al. Synthesis and characterization of single-phase epitaxial Cr 2 N thin films by reactive magnetron sputtering. 2019;54(2):1434-42

Ghazaryan, D., Greenaway, M.T., Wang, Z., Guarochico-Moreira, V.H., Vera-Marun, I.J., Yin, J., et al, 2018. Magnon-assisted tunnelling in van der Waals heterostructures based on CrBr 3. Nat. Electron. 1 (6), 344–349.

Gibertini, M., Koperski, M., Morpurgo, A.F., Novoselov, K.S., 2019. Magnetic 2D materials and heterostructures. Nat. Nanotechnol. 14 (5), 408–419.

Gong, C., Li, L., Li, Z., Ji, H., Stern, A., Xia, Y., et al, 2017. Discovery of intrinsic ferromagnetism in two-dimensional van der Waals crystals. Nature 546 (7657), 265–269.

Grönke, M., Buschbeck, B., Schmidt, P., Valldor, M., Oswald, S., Hao, Q., et al, 2019. Chromium Trihalides CrX3 (X = Cl, Br, I): direct deposition of micro-and nanosheets on substrates by chemical vapor transport. Adv. Mater. Interfaces 6 (24), 1901410.

Habib MR, Wang S, Wang W, Xiao H, Obaidulla SM, Gayen A, et al. Electronic properties of polymorphic two-dimensional layered chromium disulphide. 2019;11(42):20123-32

Han, W., Liu, K., Yang, S., Wang, F., Su, J., Jin, B., et al, 2019. Salt-assisted chemical vapor deposition of two-dimensional materials. Sci. China Chem. 62 (10), 1300–1311.

Han, H., Yu, H., Wei, H., Gong, J., Xu, W., 2019. Recent progress in three-terminal artificial synapses: from device to system. Small 15 (32), 1900695.

Heinig, N., Jalili, H., Leung, K., 2007. Fabrication of epitaxial Cr O 2 nanostructures directly on MgO (100) by pulsed laser deposition. Appl. Phys. Lett. 91, (25) 253102.

Hones P, Sanjines R, Levy FJS, Technology C. Characterization of sputter-deposited chromium nitride thin films for hard coatings. 1997;94:398-402

Huang B, Clark G, Navarro-Moratalla E, Klein DR, Cheng R, Seyler KL, et al. Layer-dependent ferromagnetism in a van der Waals crystal down to the monolayer limit. 2017;546(7657):270-3

Huang, W., Gan, L., Yang, H., Zhou, N., Wang, R., Wu, W., et al, 2017. Controlled synthesis of ultrathin 2D β-In2S3 with broadband photoresponse by chemical vapor deposition. Adv. Funct. Mater. 27 (36), 1702448.

Ingle, N., Hammond, R., Beasley, M., 2001. Growth of the Cr oxides via activated oxygen reactive molecular beam epitaxy: comparison of the Mo and W oxides. J. Appl. Phys. 89 (8), 4631–4635.

Ishibashi, S., Namikawa, T., Satou, M., 1978. Epitaxial growth of CrO2 on sapphire in air. Jpn. J. Appl. Phys. 17 (1), 249.

Ishibashi, S., Namikawa, T., Satou, M., 1979. Epitaxial growth of ferromagnetic CrO2 films in air. Mater. Res. Bull. 14 (1), 51–57.

Ito T, Ido H, Motizuki K. Electronic structure and magnetic properties in CrX (XP, As and Sb). Journal of Magnetism and Magnetic Materials. 2007;310(2, Part 2):e558-e9

Ivanov P, Watts S, Lind DJJoAP. Epitaxial growth of CrO 2 thin films by chemical-vapor deposition from a Cr 8 O 21 precursor. 2001;89(2):1035-40

Jiang S, Shan J, Mak KFJNm. Electric-field switching of two-dimensional van der Waals magnets. 2018;17(5):406-10

Jiang, S., Li, L., Wang, Z., Shan, J., Mak, K.F., 2019. Spin tunnel field-effect transistors based on two-dimensional van der Waals heterostructures. Nat. Electron. 2 (4), 159–163.

Jõgiaas, T., Tarre, A., Mändar, H., Kozlova, J., Tamm, A., 2022. Nanoindentation of chromium oxide possessing superior hardness among atomic-layer-deposited oxides. Nanomaterials 12 (1), 82.

Kang, K., Xie, S., Huang, L., Han, Y., Huang, P.Y., Mak, K.F., et al, 2015. High-mobility three-atom-thick semiconducting films with wafer-scale homogeneity. Nature 520 (7549), 656–660.

Kazim, S., Ali, M., Palleschi, S., D'olimpio, G., Mastrippolito, D., Politano, A., et al, 2020. Mechanical exfoliation and layer number identification of single crystal monoclinic CrCl3. Nanotechnology 31, (39) 395706.

Khan K, Tareen AK, Aslam M, Zhang Y, Wang R, Ouyang Z, et al. Recent advances in two-dimensional materials and their nanocomposites in sustainable energy conversion applications. 2019;11(45):21622-78

Khan, I., Hong, J., 2020. High Curie temperature and strain-induced semiconductor-metal transition with spin reorientation transition in 2D CrPbTe3 monolayer. Nanotechnology 31, (19) 195704.

Khan, K., Tareen, A.K., Aslam, M., Khan, Q., Khan, S.A., Khan, Q. U., et al, 2019. Novel two-dimensional carbon–chromium nitride-based composite as an electrocatalyst for oxygen reduction reaction. Front. Chem. 7, 738.

Kim, H.H., Yang, B., Patel, T., Sfigakis, F., Li, C., Tian, S., et al, 2018. One million percent tunnel magnetoresistance in a magnetic van der Waals heterostructure. Nano Lett. 18 (8), 4885–4890.

Kim, H.H., Yang, B., Tian, S., Li, C., Miao, G.-X., Lei, H., et al, 2019. Tailored tunnel magnetoresistance response in three ultrathin chromium trihalides. Nano Lett. 19 (8), 5739–5745.

Klein, D.R., MacNeill, D., Lado, J.L., Soriano, D., Navarro-Moratalla, E., Watanabe, K., et al, 2018. Probing magnetism in 2D van der Waals crystalline insulators via electron tunneling. Science 360 (6394), 1218–1222.

Knox KJAC. Structures of chromium (III) fluoride. 1960;13(6):507-8

Koroleva L, Khapaeva TM, Lomonosov MV. Superconductivity, antiferromagnetism and ferromagnetism in periodic table of D.I. Mendeleev. Journal of Physics: Conference Series. 2009;153:012057

Kuklin, A.V., Visotin, M.A., Baek, W., Avramov, P.V., 2020. CrI3 magnetic nanotubes: a comparative DFT and DFT + U study, and strain effect. Physica E 123, 114205.

Kumari S, Pradhan DK, Pradhan NR, Rack PDJEM. Recent developments on 2D magnetic materials: challenges and opportunities. 2021:1-20.

Lasek K, Coelho PM, Zberecki K, Xin Y, Kolekar SK, Li J, et al. Molecular beam epitaxy of transition metal (Ti-, V-, and Cr-) tellurides: from monolayer ditellurides to multilayer self-intercalation compounds. 2020;14(7):8473-84

Lee MJ, Lee S, Lee S, Balamurugan K, Yoon C, Jang JT, et al. Synaptic devices based on two-dimensional layered single-crystal chromium thiophosphate (CrPS 4). 2018;10(4):23-30

Lee IH, Choi BK, Kim HJ, Kim MJ, Jeong HY, Lee JH, et al. Modulating Curie Temperature and Magnetic Anisotropy in Nanoscale-Layered Cr2Te3 Films: Implications for Room-Temperature Spintronics. 2021;4(5):4810-9

Lenz, M., Gruehn, R., 1997. Developments in measuring and calculating chemical vapor transport phenomena demonstrated on Cr, Mo, W, and their compounds. Chem. Rev. 97 (8), 2967–2994.

Leskelä, M., Niinistö, J., Ritala, M., 2014. 4.05 - Atomic Layer Deposition. In: Hashmi, S., Batalha, G.F., Van Tyne, C.J., Yilbas, B. (Eds.), Comprehensive Materials Processing. Elsevier, Oxford, pp. 101–123.

Li X, Yang JJJoMCC. CrXTe 3 (X = Si, Ge) nanosheets: two dimensional intrinsic ferromagnetic semiconductors. 2014;2 (34):7071-6

Li, X., Gupta, A., Xiao, G., 1999. Influence of strain on the magnetic properties of epitaxial (100) chromium dioxide (CrO 2) films. Appl. Phys. Lett. 75 (5), 713–715.

Li, B., Wan, Z., Wang, C., Chen, P., Huang, B., Cheng, X., et al, 2021. Van der Waals epitaxial growth of air-stable CrSe2 nanosheets with thickness-tunable magnetic order. Nat. Mater. 20 (6), 818–825.

Li, H., Wang, L., Chen, J., Yu, T., Zhou, L., Qiu, Y., et al, 2019. Molecular beam epitaxy grown Cr2Te3 thin films with tunable Curie temperatures for spintronic devices. ACS Appl. Nano Mater. 2 (11), 6809–6817.

Li, P., Wang, C., Zhang, J., Chen, S., Guo, D., Ji, W., et al, 2020. Single-layer CrI3 grown by molecular beam epitaxy. Sci. Bull. 65 (13), 1064–1071.

Lin M-W, Zhuang HL, Yan J, Ward TZ, Puretzky AA, Rouleau CM, et al. Ultrathin nanosheets of CrSiTe 3: a semiconducting two-dimensional ferromagnetic material. 2016;4(2):315-22

Lin G, Zhuang H, Luo X, Liu B, Chen F, Yan J, et al. Tricritical behavior of two-dimensional intrinsic ferromagnetic semiconducting CrGeTe3. 2017.

Ling T, Wang JJ, Zhang H, Song ST, Zhou YZ, Zhao J, et al. Freestanding ultrathin metallic nanosheets: Materials, synthesis, and applications. 2015;27(36):5396-402

Liu, P.S., Chen, G.F., 2014. Chapter Nine - Characterization Methods: Basic Factors. In: Liu, P.S., Chen, G.F. (Eds.), Porous Materials. Butterworth-Heinemann, Boston, pp. 411–492.

Liu J, Sun Q, Kawazoe Y, Jena PJPCCP. Exfoliating biocompatible ferromagnetic Cr-trihalide monolayers. 2016;18(13):8777-84

Liu J, Yu X, Du R, Zhang C, Zhang T, Llorca J, et al. Chromium phosphide CrP as highly active and stable electrocatalysts for oxygen electroreduction in alkaline media. 2019;256:117846

Mattinen M. Atomic Layer Deposition of Two-Dimensional Metal Dichalcogenides. 2020.

McGuire MA, Dixit H, Cooper VR, Sales BCJCoM. Coupling of crystal structure and magnetism in the layered, ferromagnetic insulator CrI3. 2015;27(2):612-20

Mogi, M., Tsukazaki, A., Kaneko, Y., Yoshimi, R., Takahashi, K., Kawasaki, M., et al, 2018. Ferromagnetic insulator Cr2Ge2Te6 thin films with perpendicular remanence. APL Mater. 6, (9) 091104.

Mogulkoc A, Modarresi M, Rudenko AJPRB. Two-dimensional chromium pnictides Cr X (X = P, As, Sb): Half-metallic ferromagnets with high Curie temperature. 2020;102(2):024441

Mogulkoc A, Modarresi M, Rudenko AJPRA. Two-dimensional chromium bismuthate: a room-temperature Ising ferromagnet with tunable magneto-optical response. 2021;15(6):064053

Motojima S, Higashi TJJocg. Deposition and hallow crystal growth of CrP and Cr3P by CVD process. 1985;71(3):639-47

Mu Q-G, Ruan B-B, Pan B-J, Liu T, Yu J, Zhao K, et al. Ion-exchange synthesis and superconductivity at 8.6 K of N a 2 C r 3 A s 3 with quasi-one-dimensional crystal structure. 2018;2(3):034803

Nigro A, Cuono G, Marra P, Leo A, Grimaldi G, Liu Z, et al. Dimensionality of superconductivity in the transition metal pnictide WP. 2020.

Nikitov, S.A., Kalyabin, D.V., Lisenkov, I.V., Slavin, A.N., Barabanenkov, Y.N., Osokin, S.A., et al, 2015. Magnonics: a new research area in spintronics and spin wave electronics. Phys. Usp. 58 (10), 1002.

Ningrum VP, Liu B, Wang W, Yin Y, Cao Y, Zha C, et al. Recent advances in two-dimensional magnets: Physics and devices towards spintronic applications. 2020;2020.

Noce, C., 2020. The chromium pnictide materials: a tunable platform for exploring new exciting phenomena. EPL (Europhys. Lett.) 130 (6), 67001.

Nylund MA, Roger M, Sénateur J, Fruchart RJJoSSC. Evolution structurale des phosphures, arséniures et arséniophosphures M2P, M2As et M2 (P1− xAsx). 1972;4(1):115-22.

Och, M., Martin, M.-B., Dlubak, B., Seneor, P., Mattevi, C., 2021. Synthesis of emerging 2D layered magnetic materials. Nanoscale 13 (4), 2157–2180.

Ohta S, Kanomata T, Kaneko TJJom, materials m. Magnetic properties of CrRhAs and CrRuAs. 1990;90:171-2

Ohta S, Kaneko T, Yoshida H, Kanomata T, Yamauchi HJJom, materials m. Pressure effect on the magnetic transition temperatures and thermal expansion in chromium ternary pnictides CrMAs (M = Ni, Rh). 1995;150(2):157-64

Okamoto, Y., Fujii, M., Imanaka, T., Teranishi, S., 1976. X-ray photoelectron spectroscopic studies of catalysts—chromia–alumina catalysts—. Bull. Chem. Soc. Jpn. 49 (4), 859–863.

Ostwal, V., Shen, T., Appenzeller, J., 2020. Efficient Spin-orbit torque switching of the semiconducting Van Der Waals ferromagnet Cr2Ge2Te6. Adv. Mater. 32 (7), 1906021.

Otero Fumega A, Phillips J, Pardo VJTJoPCC. Controlled two-dimensional ferromagnetism in 1T–CrTe2: the role of charge density wave and strain. 2020;124(38):21047-53

Ouvrard G, Sandre E, Brec RJJoSSC. Synthesis and crystal structure of a new layered phase: The chromium hexatellurosilicate Cr2Si2Te6. 1988;73(1):27-32

Pei Q, Luo X, Lin G, Song J, Hu L, Zou Y, et al. Spin dynamics, electronic, and thermal transport properties of two-dimensional CrPS4 single crystal. 2016;119(4):043902

Peng Y, Ding S, Cheng M, Hu Q, Yang J, Wang F, et al. Magnetic structure and metamagnetic transitions in the van der Waals antiferromagnet CrPS4. 2020;32(28):2001200

Polesya S, Kuhn G, Benea D, Mankovsky S, Ebert HJZfauaC. Electronic structure and magnetic properties of chromium chalcogenides and pnictides with NiAs structure. 2013;639(15):2826-35

Pramanik, T., Roy, A., Dey, R., Rai, A., Guchhait, S., Movva, H.C., et al, 2017. Angular dependence of magnetization reversal in epitaxial chromium telluride thin films with perpendicular magnetic anisotropy. J. Magn. Magn. Mater. 437, 72–77.

Purbawati, A., Coraux, J., Vogel, J., Hadj-Azzem, A., Wu, N., Bendiab, N., et al, 2020. In-plane magnetic domains and Néel-like domain walls in thin flakes of the room temperature CrTe2 van der Waals ferromagnet. ACS Appl. Mater. Interfaces 12 (27), 30702–30710.

Rabe M, Pommer J, Samm K, Özyilmaz B, König C, Fraune M, et al. Growth and magnetotransport study of thin ferromagnetic CrO2 films. 2001;14(1):7

Rodríguez-de Marcos, L.V., Kalaiselvi, S.M., Leong, O.B., Das, P. K., Breese, M.B., Rusydi, A., 2020. Optical constants and absorption properties of Te and TeO thin films in the 13–14 nm spectral range. Opt. Express 28 (9), 12922–12935.

Roy A, Dey R, Pramanik T, Rai A, Schalip R, Majumder S, et al. Structural and magnetic properties of molecular beam epitaxy grown chromium selenide thin films. 2020;4(2):025001

Roy, A., Guchhait, S., Dey, R., Pramanik, T., Hsieh, C.-C., Rai, A., et al, 2015. Perpendicular magnetic anisotropy and spin glass-like behavior in molecular beam epitaxy grown chromium telluride thin films. ACS Nano 9 (4), 3772–3779.

Samadi M, Sarikhani N, Zirak M, Zhang H, Zhang H-L, Moshfegh AZJNH. Group 6 transition metal dichalcogenide nanomaterials: synthesis, applications and future perspectives. 2018;3(2):90-204

Sangwan, V.K., Lee, H.-S., Bergeron, H., Balla, I., Beck, M.E., Chen, K.-S., et al, 2018. Multi-terminal memtransistors from polycrystalline monolayer molybdenum disulfide. Nature 554 (7693), 500–504.

Shcherbakov, D., Stepanov, P., Weber, D., Wang, Y., Hu, J., Zhu, Y., et al, 2018. Raman spectroscopy, photocatalytic degradation, and stabilization of atomically thin chromium tri-iodide. Nano Lett. 18 (7), 4214–4219.

Shima, M., Tepper, T., Ross, C., 2002. Magnetic properties of chromium oxide and iron oxide films produced by pulsed laser deposition. J. Appl. Phys. 91 (10), 7920–7922.

Shivayogimath, A., Thomsen, J.D., Mackenzie, D.M., Geisler, M., Stan, R.-M., Holt, A.J., et al, 2019. A universal approach for the synthesis of two-dimensional binary compounds. Nat. Commun. 10 (1), 1–7.

Sivadas N, Daniels MW, Swendsen RH, Okamoto S, Xiao DJPRB. Magnetic ground state of semiconducting transition-metal trichalcogenide monolayers. 2015;91(23):235425

Song, T., Cai, X., Tu Matisse, W.-Y., Zhang, X., Huang, B., Wilson Nathan, P., et al, 2018. Giant tunneling magnetoresistance in spin-filter van der Waals heterostructures. Science 360 (6394), 1214–1218.

Song, T., Tu, M.-W.-Y., Carnahan, C., Cai, X., Taniguchi, T., Watanabe, K., et al, 2019. Voltage control of a van der Waals spin-filter magnetic tunnel junction. Nano Lett. 19 (2), 915–920.

Sousa, P.M., Dias, S.A., Silvestre, A.J., Conde, O., Morris, B., Yates, K.A., et al, 2006. CVD of CrO2: towards a lower temperature deposition process. Chem. Vap. Depos. 12 (12), 712–714.

Sousa PM, Dias SA, Conde O, Silvestre AJ, Branford WR, Morris B, et al. Influence of growth temperature and carrier flux on the structure and transport properties of highly oriented CrO2 on Al2O3 (0001). 2007;13(10):537-45.

Stanoi, D., Socol, G., Grigorescu, C., Guinneton, F., Monnereau, O., Tortet, L., et al, 2005. Chromium oxides thin films prepared and coated in situ with gold by pulsed laser deposition. Mater. Sci. Eng. B 118 (1–3), 74–78.

Su J, Liu K, Wang F, Jin B, Guo Y, Liu G, et al. Van der waals 2D transition metal tellurides. 2019;6(19):1900741.

Sun Y, Yan P, Ning J, Zhang X, Zhao Y, Gao Q, et al. Ferromagnetism in two-dimensional CrTe2 epitaxial films down to a few atomic layers. 2021;11(3):035138

Sun, F., Hong, A., Zhou, W., Yuan, C., Zhang, W., 2020. Prediction for structure stability and ultrahigh hydrogen evolution performance of monolayer 2H-CrS2. Mater. Today Commun. 25, 101707.

Suzuki, T., Saito, H., Hirai, M., Suematsu, H., Jiang, W., Yatsui, K., 2002. Preparation of Cr (Nx, Oy) thin films by pulsed laser deposition. Thin Solid Films 407 (1–2), 118–121.

Ta HQ, Yang QX, Liu S, Bachmatiuk A, Mendes RG, Gemming T, et al. In situ formation of free-standing single-atom-thick antiferromagnetic chromium membranes. 2020;20(6):4354-61

Tabbal, M., Kahwaji, S., Christidis, T., Nsouli, B., Zahraman, K., 2006. Pulsed laser deposition of nanostructured dichromium trioxide thin films. Thin Solid Films 515 (4), 1976–1984.

Tang, Z.-T., Bao, J.-K., Liu, Y., Sun, Y.-L., Ablimit, A., Zhai, H.-F., et al, 2015. Unconventional superconductivity in quasi-one-dimensional ${\mathrm{Rb}}_{2}{\mathrm{Cr}}_{3}{\mathrm{As}}_{3}$. Phys. Rev. B 91, (2) 020506.

Tarre, A., Aarik, J., Mändar, H., Niilisk, A., Pärna, R., Rammula, R., et al, 2008. Atomic layer deposition of Cr2O3 thin films: Effect of crystallization on growth and properties. Appl. Surf. Sci. 254 (16), 5149–5156.

Tian Y, Gray MJ, Ji H, Cava R, Burch KSJDM. Magneto-elastic coupling in a potential ferromagnetic 2D atomic crystal. 2016;3 (2):025035

Tian, H., Guo, Q., Xie, Y., Zhao, H., Li, C., Cha, J.J., et al, 2016. Anisotropic black phosphorus synaptic device for neuromorphic applications. Adv. Mater. 28 (25), 4991–4997.

Utama, M.I.B., Zhang, Q., Zhang, J., Yuan, Y., Belarre, F.J., Arbiol, J., et al, 2013. Recent developments and future directions in the growth of nanostructures by van der Waals epitaxy. Nanoscale 5 (9), 3570–3588.

Wang J, Deng S, Liu Z, Liu ZJNSR. The rare two-dimensional materials with Dirac cones. 2015;2(1):22-39

Wang F, Du J, Sun F, Sabirianov RF, Al-Aqtash N, Sengupta D, et al. Ferromagnetic Cr 2 Te 3 nanorods with ultrahigh coercivity. 2018;10(23):11028-33

Wang C, Zhou X, Pan Y, Qiao J, Kong X, Kaun C-C, et al. Layer and doping tunable ferromagnetic order in two-dimensional Cr S 2 layers. 2018;97(24):245409.

Wang, Z., Zhang, T., Ding, M., Dong, B., Li, Y., Chen, M., et al, 2018. Electric-field control of magnetism in a few-layered van der Waals ferromagnetic semiconductor. Nat. Nanotechnol. 13 (7), 554–559.

Webster L, Yan J-AJPRB. Strain-tunable magnetic anisotropy in monolayer CrCl 3, CrBr 3, and CrI 3. 2018;98(14):144411.

Wei, W.C.J., Lo, M.H., 1998. Processing and properties of (Mo, Cr) oxycarbides from MOCVD. Appl. Organomet. Chem. 12 (3), 201–220.

Xi, K., Chu, S., Zhang, X., Zhang, X., Zhang, H., Xu, H., et al, 2020. A high-performance layered Cr-based cathode for sodium-ion batteries. Nano Energy 67, 104215.

Xiao, X., Wang, H., Urbankowski, P., Gogotsi, Y., 2018. Topochemical synthesis of 2D materials. Chem. Soc. Rev. 47 (23), 8744–8765.

Xu W, Ali S, Jin Y, Wu X, Xu HJAAEM. Intrinsic Ferromagnetic Semiconductors in Two-Dimensional Alkali-Based Chromium Chalcogenides. 2020;2(12):3853-8

Yamaguchi M, Hashimoto TJJotPSoJ. Magnetic properties of Cr3Te4 in ferromagnetic region. 1972;32(3):635-8

Yang, R., Huang, H.M., Guo, X., 2019. Memristive synapses and neurons for bioinspired computing. Adv. Electron. Mater. 5 (9), 1900287.

Yuan W, Zhu Q, Su T, Yao Y, Xing W, Chen Y, et al. Experimental signatures of spin superfluid ground state in canted antiferromagnet Cr2O3 via nonlocal spin transport. Science advances. 2018;4(4): eaat1098

Zavabeti, A., Jannat, A., Zhong, L., Haidry, A.A., Yao, Z., Ou, J.Z., 2020. Two-dimensional materials in large-areas: synthesis, properties and applications. Nano-Micro Lett. 12 (1), 1–34.

Zhang W-B, Qu Q, Zhu P, Lam C-HJJoMCC. Robust intrinsic ferromagnetism and half semiconductivity in stable two-dimensional single-layer chromium trihalides. 2015;3(48):12457-68

Zhang X, Zhao Y, Song Q, Jia S, Shi J, Han WJJoAP. Magnetic anisotropy of the single-crystalline ferromagnetic insulator Cr2Ge2Te6. 2016;55(3):033001

Zhang Z, Chu J, Yin L, Shifa TA, Cheng Z, Cheng R, et al. Ultrathin magnetic 2D single-crystal CrSe. 2019;31(19):1900056.

Zhang Z, Shang J, Jiang C, Rasmita A, Gao W, Yu TJNl. Direct photoluminescence probing of ferromagnetism in monolayer two-dimensional CrBr3. 2019;19(5):3138-42

Zhao, Q., Xie, Z., Peng, Y.-P., Wang, K., Wang, H., Li, X., et al, 2020. Current status and prospects of memristors based on novel 2D materials. Mater. Horiz. 7 (6), 1495–1518.

Zhou S, Wang R, Han J, Wang D, Li H, Gan L, et al. Ultrathin non-van der Waals magnetic Rhombohedral Cr2S3: space-confined chemical vapor deposition synthesis and raman scattering investigation. 2019;29(3):1805880

Zhou, S., Gan, L., Wang, D., Li, H., Zhai, T., 2018. Space-confined vapor deposition synthesis of two dimensional materials. Nano Res. 11 (6), 2909–2931.

Zhuang HL, Johannes MD, Blonsky MN, Hennig RGJAPL. Computational prediction and characterization of single-layer CrS2. 2014;104(2):022116.

Zhuang HL, Xie Y, Kent P, Ganesh PJPRB. Computational discovery of ferromagnetic semiconducting single-layer CrSnTe 3. 2015;92(3):035407

Zhuge X, Wang J, Zhuge F. Photonic synapses for ultrahigh-speed neuromorphic computing. physica status solidi (RRL)–Rapid Research Letters. 2019;13(9):1900082